공학박사 학위논문

Nanomaterial development for heart failure prevention and cardiotoxicity evaluation

심부전 예방과 심독성 측정을 위한 나노소재 개발

2021년 8월

서울대학교 대학원

화학생물공학부

권 성 필

Nanomaterial development for heart failure prevention and cardiotoxicity evaluation

지도교수 김 병 수

이 논문을 공학박사 학위논문으로 제출함

2021년 8월

서울대학교 대학원

화학생물공학부

권 성 필

권성필의 공학박사 학위논문을 인준함
2021년 8월

위원장 황 석 연

부위원장 김 병 수

위 원 서 상 우

위 원 한 지 숙

위 원 장 기 욱

Abstract

Nanomaterial development for heart failure prevention and cardiotoxicity evaluation

Sung Pil Kwon
School of Chemical and Biological Engineering
The Graduate School
Seoul National University

Myocardial infarction (MI) can be caused by several issues, including drug-induced cardiotoxicity. Anthracycline-based anti-cancer drugs such as doxorubicin are known for provoking cardiac damage, resulting in MI and heart failure. Severe cardiac damage following MI causes excessive inflammation, which sustains tissue damage and often aggravates adverse cardiac remodeling towards cardiac function impairment and heart failure. Timely diagnosis and resolution of the inflammation may prevent the cardiac remodeling and the heart failure development.

Nanomaterials have high potential for bioapplication such as therapeutics and diagnosis. Especially, nanoparticles are widely used formulation to deliver drugs or biomolecules. The nanoformulation can be advantageous to 1) facile surface modification, 2) blocking

drug degradation by enzyme in human body, 3) interaction with cells facilitated by nanosize of the particles, all of which enable particle property control and efficient cargo delivery. Although nanomaterials seem to have many advantages and potential in heart failure prevention, nanotechnology is not much engaged in MI diagnosis and treatment.

Here, the merits of nanomaterials in MI treatment and evaluation of drug-induced cardiotoxicity are introduced. First, intradermal injection of L-Ag/R (liposomal antigen and rapamycin) enabled effective spatiotemporal co-delivery of antigens and rapamycin to DCs, improving immunotolerance and cardiac function. Second, with nanoporous, nanothin PLGA membrane-based cell culture platform, I can find a potential factor that influences on drug-induced cardiotoxicity. The platform may enhance accuracy of drug toxicity prediction. Thus, nanomaterials can contribute to predicting and preventing heart failure and provide opportunity to approach clinical application.

Keyword : Nanomaterial, Nanomedicine, myocardial infarction, drug-induced cardiotoxicity

Student Number : 2016-33931

Table of Contents

List of Tables

List of Figures

Chapter 1. Research backgrounds and objective

1.1. Research backgrounds

1.1.1 Myocardial infarction aggravated by inflammation

To prevent myocardial necrosis following myocardial infarction (MI), coronary reperfusion strategies including percutaneous coronary intervention are challenged. Nevertheless, a large proportion of MI patients develop heart failure within years, and the development of heart failure results in ~90% of mortality.[1,2] Recently, inflammation during MI have gained much attention because inflammatory response are mainly engaged in MI progression (Fig. 1.1.1). Following MI, the immune system is engaged to repair the cardiac damage. At the onset of MI, the apoptosis of cardiomyocytes triggers increase in reactive oxygen species (ROS) and damage associated molecular pattern (DAMP) abruptly, which causes a large number of neutrophils and macrophages to infiltrate and be activated.[2] The inflammatory cells remove the damaged cells and help recovery of the tissue integrity. After that, the immune balance is shifted from inflammatory to regulatory mechanism, resolving the inflammation. However, severe cardiac damage causes excessive inflammation, sustains tissue damage and aggravates adverse cardiac remodeling

towards heart failure.[2]

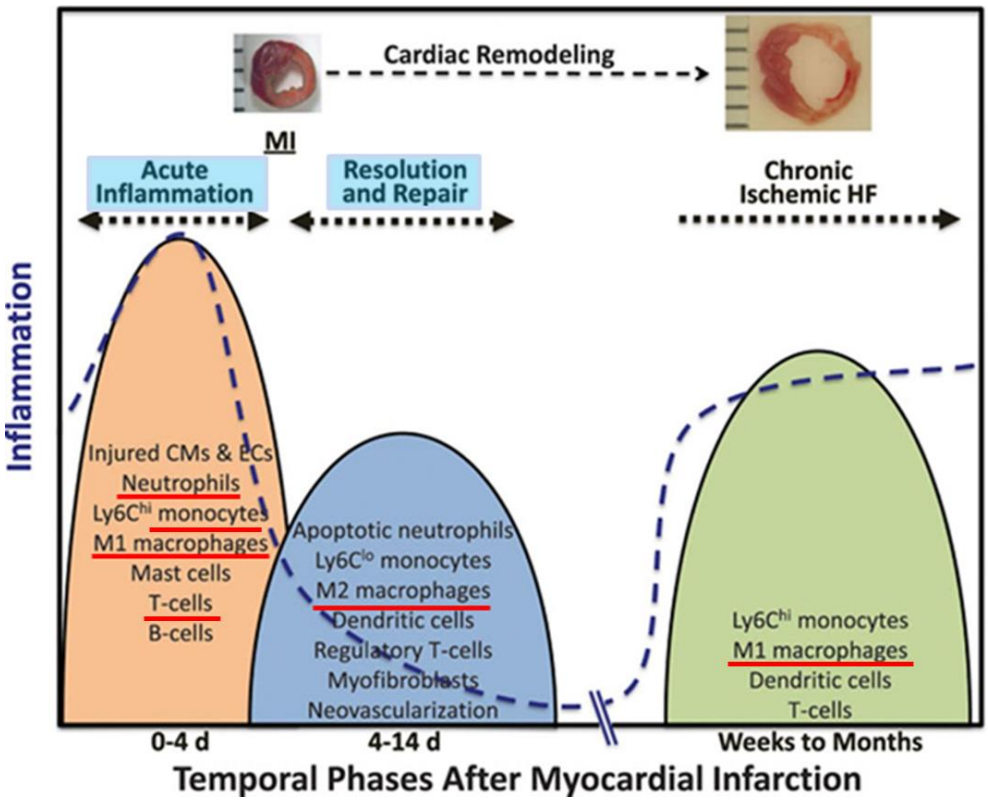

Figure 1.1.1 Progression of inflamation following myocardial infarction.[3]

1.1.2 Cell therapy for myocardial infarction and limitation

Various approaches have been investigated over the last several decades to preserve the cardiac function following MI. One of the most extensively studied approaches is mesenchymal stem cell-based therapy. However, clinical trials have failed or shown at most marginally positive outcomes.[4] To promote resolution of post-MI inflammation, adoptive cell transfer (ACT) of regulatory T cell (Treg) and tolerogenic dendritic cell (tDC) has been investigated (Fig. 1.1.2.A). Tregs can mediate immune tolerance and relieve the excessive inflammation. Tregs are engaged in post-MI healing through interactions with multiple types of cells at infarcted myocardium.[5-7] Tregs suppress activity of cytotoxic T cells and pro-inflammatory M1 macrophages,[2] ameliorating left ventricular (LV) adverse remodeling.[5] Despite the immune tolerance function of Tregs, however, off-targeted Tregs, which are not finely tuned to specific antigens, can lead to systemic immunosuppression, incurring side effects such as tumorigenesis and infection.[8] tDC, which is another key regulator of immune tolerance and induces Tregs at lymphoid tissues, can also contribute to the heart repair by inhibiting the adverse remodeling and LV function deterioration. Previous study has demonstrated that ACT of tDCs pulsed with MI tissue lysates to MI mice can induce MI-specific Tregs, improving the cardiac

remodeling and function.[5] However, ACT of ex vivo-generated Tregs or tDCs often requires extra complements such as IL-2 after administration, otherwise, lose their anti-inflammatory phenotype and tolerogenic activity.[9,10] Even more, the ex vivo preparation of tDCs is even not standardized.[10] In addition, ex vivo preparation of Tregs or tDCs for the therapy is costly, laborious, and time consuming (Fig. 1.1.2.B). Thus, there remains an unmet need for clinically facile alternatives to ACT of Tregs or tDCs.

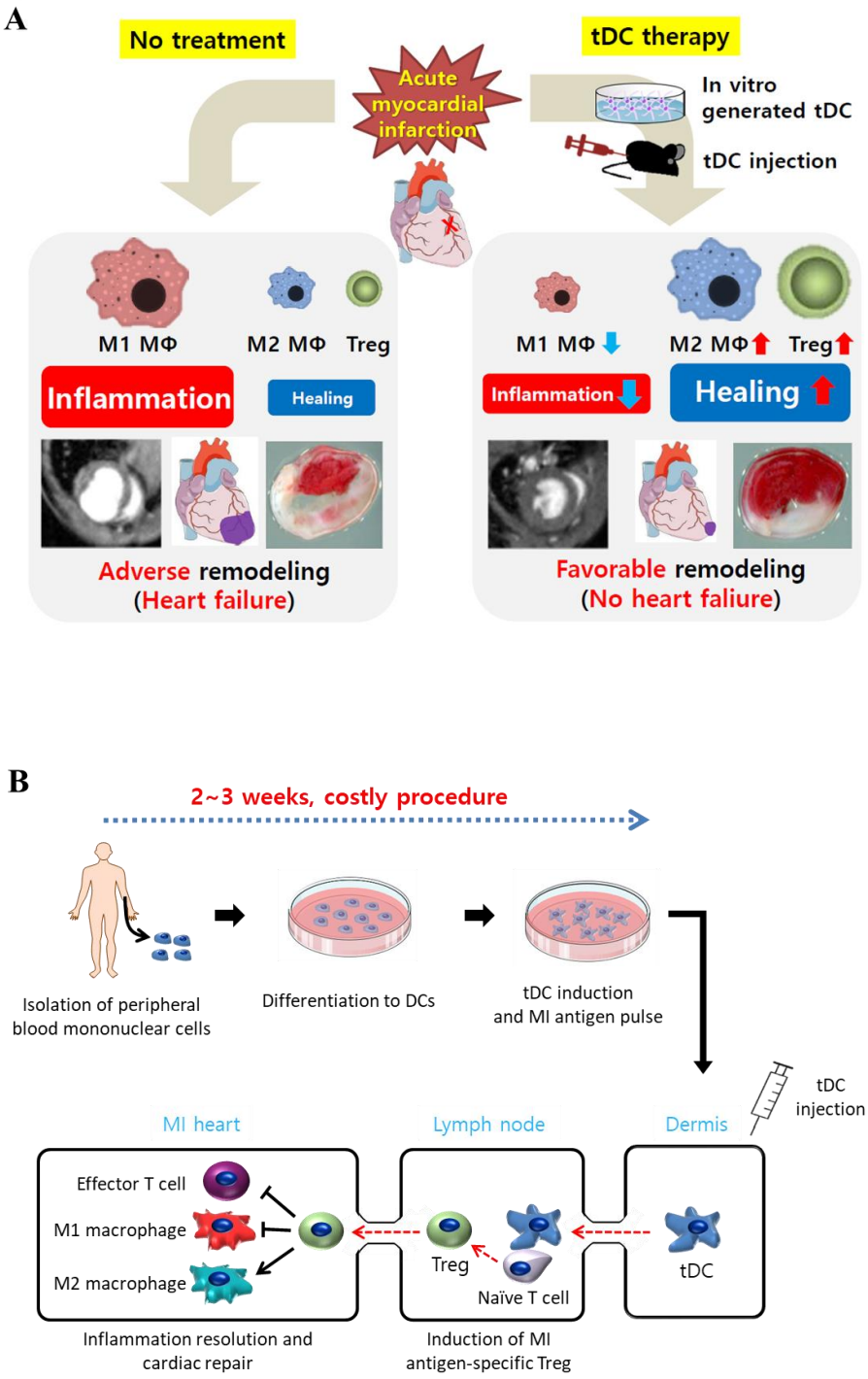

Figure 1.1.2 A) Adoptive transfer and therapeutic effects of tolerogenic dendritic cells following myocardial infarction.[5] B)

Procedure and demerit of cell transfer therapy.

1.1.3 Direct reprogramming using cardiac-mimetic environment

Direct reprogramming from fibroblasts to cardiac cells can be an attractive strategy because fibroblasts can be acquired easily with low cost. Direct reprogramming from the fibroblasts derived from patients can evade immunological issues, the potential risk of tumorigenesis, and the ethical issued in embryonic stem cell-based research. In our previous studies,[11,12] cardiac-mimetic system was developed using nanoporous, nanothin PLGA membrane and shown that the system can efficiently induce cardiac cells (Fig. 1.1.3). The culture system provides in vivo environment cardiac cues such as direct cell-cell contact and electric stimulation during direct reprogramming of fibroblasts.

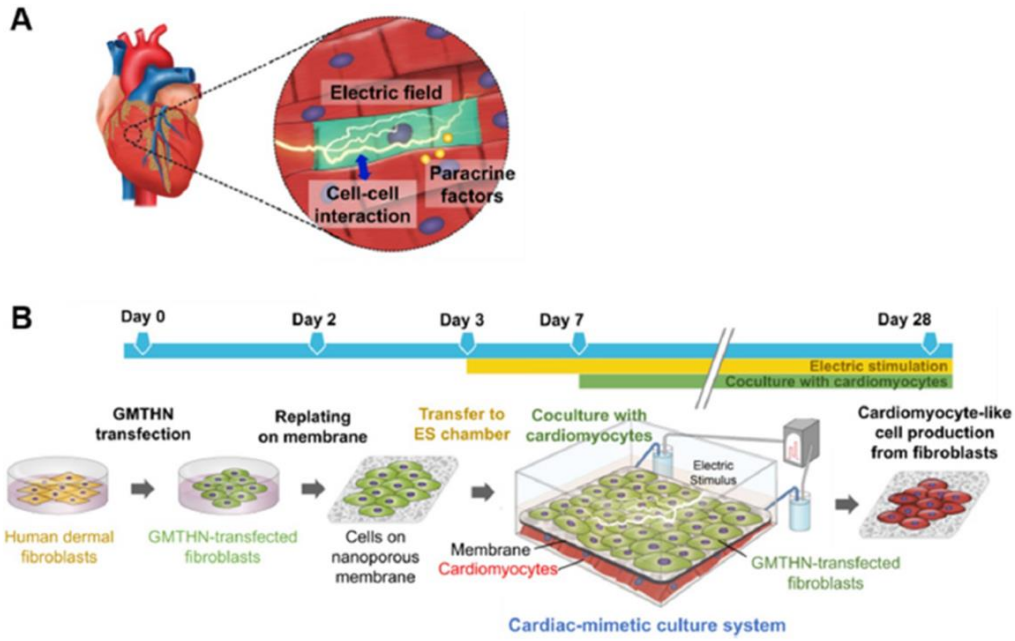

Figure 1.1.3 Cardiac-mimetic culture system.[12] A) In vivo cardiac microenvironment. B) Schemitic illustration of culture design of in vitro cardiac-mimetic culture system that mimics the cardiac microenvironment.

1.1.4 Evaluation of drug-induced cardiotoxicity

Drug-induced cardiotoxicity risks of life of cancer survivors, and its high occurrence rate is quite demanding accurate diagnosis of cardiotoxicity triggered by anti-cancer drugs.[13,14] In recent, different approaches to evaluate drug-induced cardiotoxicity have been investigated such as the use of induced pluripotent stem cell derived cardiomyocytes, cardiac cell line, and heart organoid (Table. 1.1.4). However, in vitro culture system hardly represent physiological and pharmacologic in vivo factors such as hormones, structure, cell composition in the heart, and neurohumoral influences, which can be indirectly harmed by drugs.[13] This interrupt acquiring reliable drug responsiveness data and cardiac safety liability. The lacking comprehensive knowledge in potential factors that affect drug toxicity can make waste of cost and time in preclinical trial, even delaying drug development.[15] To obtain precise in vitro data, diverse toxicity-related factors should be considered.

Construct	Composition and Description	Advantages	Disadvantages
Single hiPSC-CMs	May be micropatterned to form rectangles resembling adult myocytes	Amenable to electrophysiological studies using patch-clamp approaches	No intercalated disk or gap junctions No syncytium function Shape does not equal maturation Single-cell isolation from sheets may cause injury
2D layers	Cardiomyocytes grown in plates or wells in culture Thin film/layers or sheet constructs possible	Ease of preparation Amenable to HTS for electrophysiological, Ca flux, syncytial functions, measures of impulse propagation, fibrillation arrhythmias Cells can be matured by media, patterning extracellular matrix manipulation	Lacks influence of other cardiac cell types and 3D environment of native tissue Variable morphology and sarcomere alignment elicit strain patterns different from native myocytes
2D cocultures	hiPSC-CMs mixed with fibroblasts, vascular cells, mesenchymal stem cells, native adult cardiomyocytes	Mimics heterogeneous cellular composition of native heart Study cell-cell interactions, integrate hiPSCCMs with noncontractile cells Promotion of hiPSC-CM maturation	Optimum proportions of cell types uncertain Proliferative cells may affect preparation stability and reproducibility Nonmyocyte-to-myocyte coupling may differ from normal tissues
3D organoids	hiPSCs cocultured with fibroblasts/endothelial cells with self-assembly	Mimic 3D cardiac environment Heterogeneous cell types may resemble native heart composition	Spatial arrangements of elements uncertain Difficult to assess electrophysiology and contractility effects with multielectrode arrays and force measures
Engineered human tissues	hiPSC-CMs with/without fibroblasts, endothelial cells	Ability to directly measure contractile force, transmembrane potentials Pacing controls rate More natural alignment of cells/sarcomeres Enhanced myocyte maturation	Initial high myocyte requirements and costs being reduced by miniaturization Lack of vasculature for thicker preparations may create diffusion barrier, anoxic core Low to moderate throughput
3D macroscopic constructs	Ventricular pouches Potential mini-ventricles	Direct pressure measurements possible May promote myocyte maturation	Technically demanding, high cell quantities needed Limited to a few laboratories; low throughput; cost prohibitive

Table 1.1.4 Human relevant myocyte model for in vitro stuies.[13]

1.2. Research objective

To inhibit or predict heart failure, nanomaterials were introduced.

First, we developed a nanoparticle capable of modulating the immune balance toward tolerance and attenuated post-MI excessive inflammation via simple intradermal injection of the nanoparticles (Fig. 1.2.1). Liposomal nanoparticles loaded with MI-associated antigens and rapamycin (L-Ag/R) were able to elicit an antigen-specific immune tolerance in vivo by generating antigen-specific Tregs and modulating macrophage polarization in the infarct region and improve cardiac remodeling and function after acute MI. Antigen delivery by the nanoparticles achieved an augmented, durable presentation of antigens by dendritic cells (DCs). Co-delivery of antigens and rapamycin by the nanoparticles enabled antigen presentation by tDCs and subsequent induction of antigen-specific Tregs. Antigen-specific Tregs generate more effective and precise immune tolerance and higher localization at antigen-specific inflammation region than polyclonal Tregs and avoid the risk of non-specific, systemic immunosuppression by polyclonal Tregs.[8] Unlike preparation of Tregs or tDCs for ACT, L-Ag/R preparation is facile and cost-effective.

Second, we studied influence of cell density on drug responsiveness

and measured cardiotoxicity using previously invented cardiac-mimetic cells directly reprogrammed on nano-porous PLGA film (Fig. 1.2.2). The double-layered cell sheets, which was built by stacking cardiac mimetic cells on the PLGA film through layer by layer technique, were treated with 5-FU, FDA-approved anti-cancer drug. The double-layered cell showed inhibitory effects of apoptosis, lipid peroxidation, and expression of senescence and inflammatory-associated factors compared to monolayered culture. In addition, high content analysis (HCA) assay showed cardioprotective effects of double-layered cell sheet to mitochondrial membrane potential and cell membrane permeability, which demonstrated that 3D structured organization can lower drug-induced toxicity. Using the platform that can induce cardiac-mimetic cells and make multiple-layered cell sheets, this study suggests 3D structure as potential factors which should be considered when measuring drug-induced toxicity.

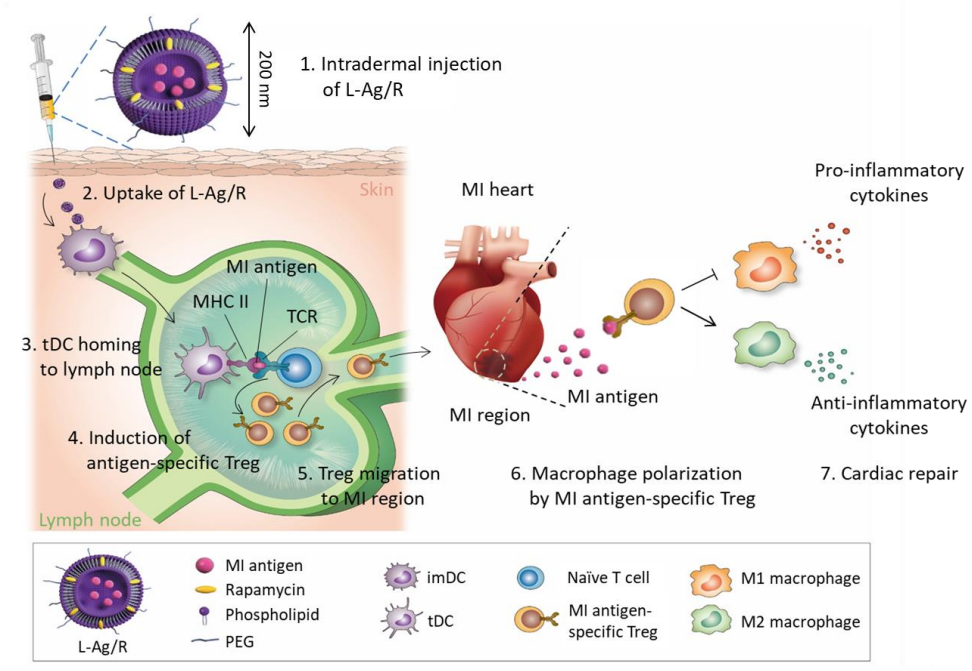

Figure 1.2.1 Nanoparticles for eliciting immunotolerance and preventing heart failure.

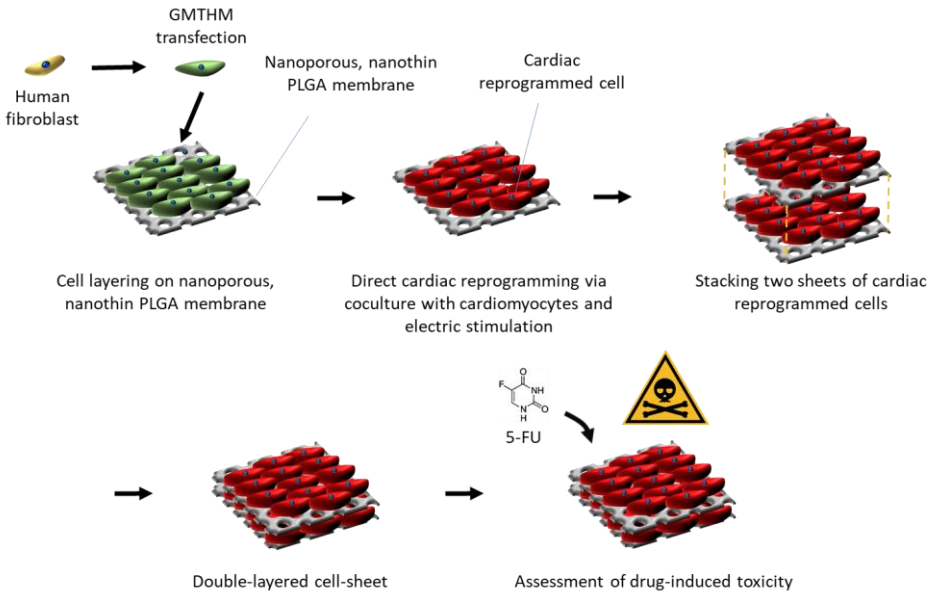

Figure 1.2.2 Evaluation of drug-induced cardiotoxicity using nanoporous, nanothin PLGA membranes.

Chapter 2. Experimental section

2.1. Preparation of nanomaterials

2.1.1. Preparation of immune-modulating nanoparticles

Synthesis procedure for the particles used in these experiments was following a conventional thin film hydration method. Briefly, DOTAP:DOPE:cholesterol:DSPE-PEG2000 lipids organic solution was constructed with molar ratio of 0.475:0.35:0.125:0.05. When L-R and L-Ag/R were formulated, 2 mol% of rapamycin was added. Then, the mixed solution was evaporated to make a lipid thin film and dried at 37 ℃ for further solvent removal. The thin film was hydrated for 1 h at 37 ℃ in 10 mM PBS (pH 7.4) with or without cardiac related antigen equivalent to 10 wt% of the phospholipids. The resulting particle solution was serially extruded through 1000, 400, 200 nm pore membranes.

2.1.2. Particle characterization

The size distribution and zeta potential were assessed with dynamic laser scattering and electrophoresis (Zetasizer Nano ZS, Malvern Panalytical, UK). To confirm colloidal stability of L-Ag/R, the particles were suspended and incubated at 37 ℃ for 144 h in PBS or

10% FBS solution. The morphology of L-Ag/R was visualized with transmission electronic microscopy (Talos L120C, FEI, Czech). L-Ag/Rs, which were previously placed onto carbon-coated copper grid, were stained with 1% (w/v) uranyl acetate, and the images were obtained with 120 keV of operating voltage. The lamellarity of L-Ag/R was verified with 31P-NMR (AvanceIII-500, Bruker, Germany). The samples were prepared by mixing the particle solution in PBS (pH 7.4) and D2O with a ratio of 9:1 (v/v), and the 31P-NMR spectra were recorded with 256 scan, 2,050 receiver gain and 13 μsec of 90° pulse width. To offset the characteristic NMR peak by phosphorus in liposomes, 5 mM of Mn2+ (MnCl2, Sigma-aldrich) were added. To evaluate contents of antigen in L-Ag and L-Ag/R, bicinchonic acid (BCA) protein assay was performed after the nanoparticle formulation was disrupted by 1 % of Triton-X 100 solution, and the absorbance at 562 nm was measured. High performance liquid chromatography (HPLC) was used for assessing the contents of rapamycin in L-R, L-Ag/R with 3:7 ratio of H2O and acetonitrile (ACN) solution as eluent. For confirming the incorporation of rapamycin and the entrapment of antigen in liposome, differential scanning calorimetry and thermogravimetric analysis was performed with thermal analyzer (TA SDT Q600, TA instruments, USA). To form free rapamycin crystal, rapamycin solution was

evaporated and subsequently hydrated. Then, lyophilized rapamycin crystal was used for the thermal analysis. The prepared L, L-R and L-Ag/R were also lyophilized, then, placed in alumina pan (Yeonjin, Seoul, Korea). The samples were heated at a rate of 10 ℃/min from 20 ℃ to 300 ℃ for DSC analysis. The amount of rapamycin prepared with different formulation (L-R, L-Ag/R and free rapamycin form) was adjusted to 0.5 mg, which was enough amount to detect presence of rapamycin. For the validation of co-localization of antigen and liposome, each of them were labelled with fluorescein isothiocyanate (FITC) and 1,1'-dioctadecyl-3,3,3',3'-tetramethylindodicarbocyanine, 4-chlorobenzenesulfonate salt (DiD), respectively. NHS-Fluorescein (Thermofisher Scientific, MA, USA) was reconstituted to make 10 mg/ml in DMSO, and was added to 2 mg/ml of antigen solution in PBS (pH7.4) with 1:20 weight ratio of FITC and the antigen. The mixed solution was stirred for 2 h with 300 rpm and room temperature. The solution was centrifuged with 14,000 g for 10 min to remove free FITC aggregate, followed by SephadexTM G-25 M (GE Healthcare, IL, USA) column gel filtration for additional purification. The concentration of the FITC-labelled antigen was calculated with BCA assay, and final yield was ~ 90 % compared to starting content of the antigens. DiD, which is favorably incorporated in liposome bilayer, was inserted in the bilayer through

addition of DiD equivalent to 1 wt.% of the lipid mixture to lipid blend solution, followed by solvent evaporation. The DiD-contained lipid thin film was hydrated with FITC-labelled antigen solution and serially extruded through 1000, 400, 200 nm pore membranes. The prepared two distinct fluorescent dye-labelled L-Ag/Rs were mounted onto cover glass, and the image was obtained by confocal microscopy: ex/em was 488/520 for FITC and 633/650 for DiD. Fluorescence resonance energy transfer (FRET) was performed to prove a close proximity of the antigens and the lipid nanoparticles. DiI up to 3.5 wt.% of the lipid mixture was added to the lipid blend before hydration and DiI-incorporated lipid thin film was hydrated with the solution containing FITC-labelled antigens. The emission spectra was obtained with 470 nm of excitation wavelength using fluorometer (Infinite 200 pro, TECAN, CH)

2.1.3. Preparation of PLGA membranes

Nanoporous, nanothin PLGA thin membranes were manufactured using PLGA spin coating method, as reported previously.[11,12] Briefly, PLGA solution was prepared by dissolving PLGA (lactide:glycolide (75 : 25), molecular weight (66,000−107,000), Sigma Aldrich) in tetrahydrofuran (Sigma Aldrich) 4 % (w/v) concentration. The PLGA solution was dropped to silicon wafers and spun at 1000 rpm for 25 s. After detachment of PLGA membranes from the silicon wafer, the membranes were framed on rectangular polyethylene terephthalate frame.

2.1.4. PLGA membrane characterization

The PLGA membranes were analyzed by tapping−mode atomic force microscopy (AFM; JPK, Nanowizard3, Germany).

2.2. Cardiac-mimetic cell reprogramming

2.2.1. Cardiac-mimetic cell culture

The cardiac transcriptional factors (Human Gata4, Mef2c, Tbx5, Hand2, Myocd; GMTHM) were subcloned into pBI-MCS-EGFP to construct plasmid. HNDFs were transfected with the cardiac transcriptional factors.[11,12] Briefly, HNDFs were washed, trysinized, and suspended at 107 cells/ml in resuspension buffer. HNDFs were mixed with the plasmid and applied an electrophoresis with a pulse of 1700 V for 20 ms (Neon® Transfection System, Invitrogen, CA, USA). The transfection efficiency was analyzed using microscope and flow cytometry (BD FACSCanto™ II Cell Analyzer, BD Biosciences, USA) 2 days after transfection. After 7 days of GMTHM transfection, markers of cardiac development stage were analyzed with qRT-PCR.

The cardiac-mimetic cell culture system was utilized to directly reprogram HNDFs to cardiac cells.[11,12] Two days after transfection, GMTHM-transfected cells were plated on the PLGA membranes, and the PLGA membranes were transferred to electric stimulation (ES) chamber, which was described in our previous report.[11,12] HL-1 cells were cultured on the ES chamber a day before coculture. After 20 days of coculture and ES, two of the PLGA membranes containing

the cardiac-mimetic cells were stacked through LbL method and incubated for 7 days to organize double-layered cell sheet. After double-layered cell sheet construction, mRNAs of cardiac markers were analyzed with qRT-PCR.

2.2.2. Double-layered cell sheet construction

After 20 days of coculture and ES, two of the PLGA membranes containing the cardiac-mimetic cells were stacked through LbL method and incubated for 7 days to organize double-layered cell sheet.

2.3. in vitro assay

2.3.1. Antigen presentation of dendritic cells

To assess antigen distribution in DCs, DCs were incubated with FITC-labelled Ag/R or FITC-labelled Ag-encapsulating L-Ag/R. After 2 h free fluorescence-labelled Ag/R or fluorescence-labelled L-Ag/R treatment, DCs were washed thoroughly and incubated for 6 h, 24 h and 48 h, respectively. Lysosomes in DCs were stained with Lysotracker Red DND-99 (Invitrogen, CA, USA) according to manufacturer' s protocol, followed by Hoechst 33342 (Sigma-aldrich) staining and image acquisition using confocal microscopy. L-Eα52-68/R were prepared similar to L-Ag/R formulation method. DCs were incubated for 2 h with free Eα52-68 (AnaSpec, CA, USA)/R or L-Eα52-68/R, followed by thorough washing. The DCs were further incubated up to 6 h, 24 h, and 48 h, respectively. The DCs were stained with Yae monoclonal antibody (eBioscienceTM) and Streptavidin APC conjugate (eBioscienceTM) subsequently. The prepared samples were analyzed with flow cytometry and confocal microscopy.

2.3.2. Induction of tolerogenic dendritic cells

Bone marrow derived DCs were generated from the well-known Lutz method[16] with some modifications. Briefly, mouse femur and tibia were dissected and flushed out bone marrow cell. 2 x 10^5 cells/ml of bone marrow cells were cultured in complete RPMI 1640 medium supplemented with 20 ng/ml mouse recombinant GM-CSF, 50nM 2-mercaptoethanol, 10% fetal bovine serum and 1% penicillin/streptomycin. At day 3, equal volume of the medium was replenished. At day 10, non-adherent cells in the culture medium were harvested by gentle pipetting and used for further experiments. For identifying capability of each nanoparticle formulation to generate tDCs, DCs were treated with 4 ug/ml L-Ag, L-Ag/R and PBS for 48 h and additional 24 h with 500ng/ml LPS for further maturation except imDC group. To validate expression of surface molecules on tDC, the induced tDCs were stained with anti-CD11c (Biolegend, CA, USA), anti-CD40 (Biolegend, #124609), anti-CD80 (Biolegend, #104705) and anti-CD86 (Biolegend, #159203), respectively, and FACS analysis was carried out. For evaluating mRNA levels of CCR7, IDO, pro- and anti-inflammatory cytokines of tDC, PCR analysis was conducted. RNA was extracted using QIAzol Lysis Reagent (Qiagen, Hilden, Germany) and used to synthesize cDNA using PCR PreMix

(Bioneer, Daejeon, Korea). qRT-PCR was performed using TOPreal™ qPCR 2X PreMIX (Enzynomics, Daejeon, Korea). The obtained data were normalized by GAPDH expression. To confirm suppressive function of T cell proliferation by tDCs generated from L-Ag/R, OT-II mice and $OVA_{323-339}$ peptides (AnaSpec) were introduced. DCs were treated with each group (equivalent to 400 ng/ml of $OVA_{323-339}$ and 20 nM rapamycin) for 2 h and an additional 500 ng/ml LPS treatment for 1 h. OT-II CD4 T cells, which were isolated using MojoSort™ Mouse CD4 T Cell Isolation Kit (Biolegend) according to the manufacturer's protocol, were labelled with carboxyfluorescein diacetate succinimidyl ester (CFSE) cell division tracker kit (Biolegend, cat# 423801). The previsously prepared DCs were co-cultured with the CFSE-labelled OT-II CD4 T cells with a ratio of 1:10. On day 4, non-adherent cells were harvested and stained with anti-CD3 (Biolegend, #100221), anti-CD4 (Biolegend, #100411), and the cell proliferation was evaluated with flow cytometry.

2.3.3. Induction of regulatory T cells

OVA-specific Tregs were induced with the same co-culture of OT-II CD4 T cells with the tDC as prepared above. 10^5 cells/ml of free OVA/R or L-OVA or L-OVA/R treated DC were cultured with 10^6 cell/ml of the OT-II CD4 T cells for 5 days. The samples were stained with anti-CD4 (Biolegend, #100437), anti-Foxp3 (Biolegend, #126403) using FOXP3 Fix/Perm buffer set according to manufacturer' s protocol and were subsequently analyzed with flow cytometry.

2.3.4. Double-layered cell structure organization

Before fabricating double-layered cell sheet, each cell sheets were labelled with 1,1'-dioctadecyl-3,3,3',3'-tetramethylindodicarbocyanine, 4-chlorobenzenesulfonate salt (DiD, Invitrogen) or 3,3'-Dioctadecyloxacarbocyanine Perchlorate (DiO, Invitrogen) for 2 h, then washed, and stacked. After 7 days, the side-view images of the double-layered cell sheet were obtained with confocal microscopy (LSM710, Carl Zeiss, Germany) installed at the National Center for Inter-university Research Facilities(NCIRF) at Seoul National University.

Mono- and double-layered cell sheets were fixed with 4% PFA at room temperature for 20 min and washed with PBS. The cell sheets

were subsequently embedded in OCT compound (Scigen, USA). The frozen blocks were sectioned at 8 μm thickness for cross-sectional observation. The sections were stained with H&E. The images of cell sheets were acquired with a microscope (IX71, Olympus, Japan). The thickness of the sheets was measured using ImageJ.

2.3.5. Apoptosis assay

5-FU treated cells were washed with PBS and trypsinized. The detached cells were stained with Apoptosis detection kit (Biolegend, CA, USA) according to manufacturer' s protocol. The samples were analyzed with flow cytometry. Bcl-2/Bax ratio was calculated by mRNA analysis

2.3.6. Lipid peroxidation assay

Cardiac-mimetic cells plated on sheets or culture dish were washed with PBS 72 h after 5-FU treatment. The cells were stained with 1 μM of C11-BODIPY (Cayman Chemical, MI, USA) for 1 h. The stained cells were detached and analyzed with flow cytometry. To obtain confocal microscopic images, the cells were stained with 1 μM C11-BODIPY and 1 μM hoechst 33342 (Sigma-Aldrich), fixed with 1 % PFA for 20 min, and analyzed with confocal microscopy.

2.3.7. Cell viability assay

Cardiac-mimetic cells, which were treated with different concentration of 5-FU, were washed with PBS, and incubated for 1 h with 10 %(v/v) EZ-Cytox solution (DoGen, Seoul, Korea) at 37 °C. The prepared samples were analyzed using microplate reader with 450 nm of excitation wavelength. (n = 3 per group)

2.3.8. Senescence and inflammatory gene expression

Senescence- (p16) and inflammatory- (TNF-a, IL-8) associated gene expression was analyzed with qRT-PCR (n = 3 per group).

2.3.9. High content analysis

Mono- and double-layered cell sheets were incubated for 72 h with different concentration of 5-FU (0, 100 nM, 1000 nM, 1 μM, 10 μM, 100 μM, and 1000 μM). Each samples were prepared with triplicate. The sheets were washed twice with PBS and incubated for 1 h with 50 nM tetramethylrhodamine ethyl ester, perchlorate (TMRE), 1 μM thiazole red homodimer (TOTO-3), and 1 μM hoechst 33342. The samples were washed 3 time with PBS and analyzed with INCell analyzer (INCell 2000, GE Healthcare, USA). Filter pairs were composed of DAPI, Cy3, and Cy5 (QUAD1). The drug responsive

curve was plotted by using GraphPad Prism software.

2.4. in vivo assay

2.4.1. Myocardial infarction operation

All animal experiments procedures were conducted in accordance with the Laboratory Animals Welfare Act, the Guide for the Care and Use of Laboratory Animals and the Guidelines and Policies for Rodent Experiments provided by the Institutional Animal Care and Use Committee (IACUC) in the School of Medicine of The Catholic University of Korea. The animal study was approved by the IACUC(CUCM-2018-0035-07). C57BL/6 mice (male, 7-8 weeks old) were anesthetized by intraperitoneal injection of a mixture of zoletil (30 mg/kg; Zoletil 50®, Virbac, France) and xylazine (10 mg/kg; Rompun®, Bayer HealthCare, Leverkusen, Germany), endotracheally intubated with a catheter (BD Angiocath Plus 22GA, BD Biosciences, Mississauga, Canada), and maintained under general anesthesia using a mechanical ventilator (Harvard Apparatus, MA, USA). The heart was exposed through a left-sided thoracotomy between the 2nd and 3rd ribs, and MI was induced by ligation of the left anterior descending artery. After MI induced, L-Ag/R nanoparticles in 100 ul PBS were injected intradermally to the left inguinal Lymph node.

2.4.2. Antigen delivery to lymph node

Cy5.5-labelled antigens were prepared similar to FITC labelled-antigens as described above. Briefly, Cy5.5-NHS ester (Lumiprobe, MD, USA) was reconstituted in DMSO, and was added to the antigen solution in PBS (pH7.4) with 1:20 weight ratio of Cy5.5 and the antigen. The mixed solution was stirred for 2 h with 300 rpm and room temperature. Centrifugation with 14,000 g for 10 min was performed to remove free Cy5.5 aggregate, followed by SephadexTM G-25 M (GE Healthcare, IL, USA) column gel filtration for additional purification. Isolated yield was ~ 85 % compared to starting content of the antigens. The fluorescent lipid nanoparticles were formulated with hydration buffer containing 0.2 mg/ml Cy5.5-labelled antigens. For tracking of L-Ag/R, Cy5.5 labeled L-Ag/R was intradermally injected near the left inguinal lymph node. After a day of administration, ex vivo images were obtained using an IVIS imaging system (IVIS Lumina XRMS, PerkinElmer, MA, USA). Prior to the dissection, mice were perfused with 10 mL of PBS, and major organs, including lung, liver, spleen, heart, kidney, and inguinal lymph nodes, were extracted. All image analyses were obtained with an IVIS imaging software (Living Imaging, PerkinElmer, MA, USA).

2.4.3. Systemic induction of immunotolerance

After 5 days of nanoparticle treatment, inguinal lymph nodes and spleens of mice treated with each particle group were extracted, minced and stained with anti-CD4, anti-CD25, and anti-Foxp3 for flow cytometry analysis.

2.4.4. Immunostaining and mRNA analysis at heart

Sample were prepared 5 days after particle administration. Tissue sections were incubated in 0.3 % H_2O_2 for 10 min at room temperature. Antigen retrieval was performed with 1 % bovine serum albumin (BSA) and 0.3 % TritonX-100 for 1 h at room temperature. The sections were incubated with primary antibodies, anti-CD11c (Biolegend, #117306), anti-CD68 (Abcam, ab53444), anti-iNOS (Abcam, ab115819), anti-CD206 (Abcam, ab64693), anti-CD31 (Abcam, ab28364) or anti- FoxP3 (Cell signaling, #12653) overnight at 4 °C. The sections were further incubated with Alexa-488 or Alexa-594-conjugated secondary antibodies (Invitrogen) for 1 h at room temperature. For terminal deoxynucleotidyl transferase dUTP nick end labeling (TUNEL) staining, we used the in situ apoptosis detection kit (TRIVIGEN, #4812-30-K). After nuclei were counterstained with DAPI, fluorescence-labeled immunostained slides were visualized by a confocal microscope (LSM;

Zeiss, Jena, Germany). All data were analyzed using ImageScope (Leica). Pro-inflammatory and anti-inflammatory cytokine-related markers were analyzed with qRT-PCR.

2.4.5. Cardiac function evaluation

Echocardiography was performed at 28 days after MI using an Affiniti 50 Imaging system (Philips, Eindhoven, Netherlands). All mice were imaged under light sedation with 1 % isoflurane to maintain a stable heart rate during echocardiographic image acquisition. The left ventricle ejection fraction (LVEF), left ventricle fractional shortening (LVFS), and left ventricle end systolic volume (LVESV) were obtained with M-mode tracing at the level of the papillary muscle.

The dissected hearts were fixed in 4 % paraformaldehyde (PFA), embedded in paraffin, and cut into 5-μm-thick serial sections using a microtome (RM2235; Leica Microsystems Inc., Mannheim, Germany). Masson' s trichrome stain were performed for infarct size and myocardial fibrosis evaluation. Infarct size were calculated as a percentage of total infarct circumference divided by total LV circumferences, in which both circumferences were obtained by midline length measurement.

2.5. Statistical analysis

All statistical analysis was performed using GraphPad Prism software (GraphPad, San Diego, CA, USA) and presented as a mean ± standard deviation (SD). Statistical significance was determined using unpaired t-test and one-way ANOVA followed by Newman-Keuls multiple comparison test. *P\0.05, **P\0.01, and #P\0.001 were considered statistically significant.

Chapter 3. Immune-modulating nanoparticle for prevention of heart failure following myocardial infarction

3.1. Nanoparticle characterization

The liposomes were prepared with conventional lipid thin film formation and hydration method. The formulated particles encapsulating both infarct myocardium lysate and rapamycin (L-Ag/R) showed ~200 nm size with spherical morphology analyzed by dynamic laser scattering (DLS) and transmission electron microscopy (TEM) (Fig. 3.1.A,B). To verify the nanostructure and lamellarity of the particle, 31P-NMR spectra of the nanoparticle were recorded (Fig. 3.1.C). Characteristic NMR peak of phosphorus in lipid bilayer appeared, in the absence of manganese ion, However, after the addition of Mn2+, which interact with the outermost phospholipids and reduced NMR signal, the sharp peak disappeared totally, suggesting that the lamellarity of the L-Ag/R nanoparticles were unilamellar.[17] The incorporation of rapamycin in L-Ag/R was also revealed by differential scanning calorimetry (DSC) (Fig. 3.1.D).

The thermogram obtained from the hydrated free rapamycin after lyophilization showed an endothermic peak ~180 °C indicating that rapamycin crystal formed,[18] in contrast, the peak was not detected in rapamycin encapsulated liposome (L−R) and L−Ag/R, as in blank liposome (L). The DSC data demonstrated that rapamycins were incorporated into liposomes and existed in an amorphous state in the lipid bilayer.[17] To reinforce Ag entrapment in liposomes, we employed a cationic lipid, DOTAP, which can strongly attract negative charged regions of Ag due to its highly positive trimethylammonium group. After fluorescein isothiocyanate (FITC) fluorescent dye labelled Ags were hydrated with a lipid film containing DiI, fluorescence resonance electron transfer (FRET) was analyzed (Fig. 3.1.E). As the DiI concentration in the nanoparticles increased, the intensity of FITC decreased, which occurred by electron transfer between DiI and FITC (electron acceptor and donor), suggesting that lipid bilayers and MI−antigens were closely contact. After FITC−labeled Ags were hydrated with a lipid film containing DiD, a lipophilic fluorescent dye, followed by sequential size extrusion, confocal microscopic examination was then performed showing that the antigens and liposomes were colocalized visually (Fig. 3.1.F). In addition, super−resolution microscopy observation showed that the antigens were distributed along the lipid nanoparticles (Fig. 3.1.G).

The particle stability of L−Ag/R over time lapse or lyophilization was assessed using DLS. The Z−average diameter of L−Ag/R was remained around ~200 nm for up to 7 days, both in PBS and in 10 % FBS (Fig. 3.1.H).

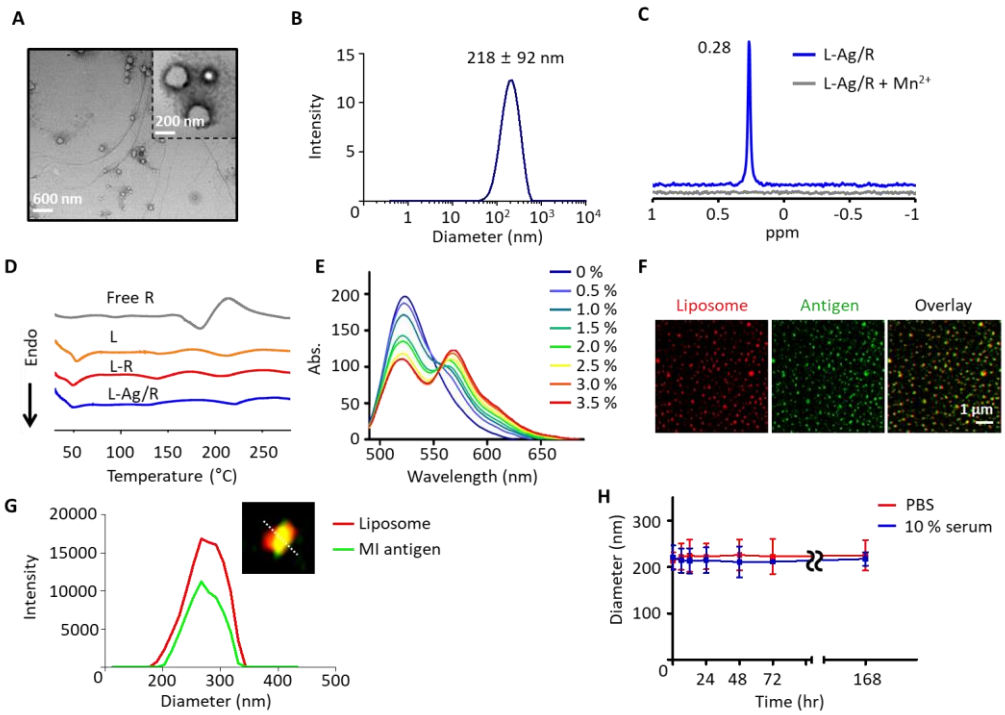

Figure 3.1. Characterization of L-Ag/R. **A)** TEM images of L-Ag/R. **B)** Size distribution of L-Ag/R. **C)** ^{31}P-NMR analysis showing that L-Ag/R is a unilamellar liposome. **D)** DSC analysis showing incorporation of rapamycin in L-R and L-Ag/R. **E)** FRET analysis showing close proximity of FITC-labeled MI antigens and DiI-labeled liposomes in L-Ag/R. **F)** Confocal microscopic images showing colocalization of FITC-labeled MI antigens (green) and DiD-labeled liposome (red) in L-Ag/R. **G)** FITC-labeled antigen distribution in DiD-labeled liposome in L-Ag/R, analyzed with super resolution microscopy. **H)** Size stability of L-Ag/R in PBS (pH 7.4) and 10 % serum in PBS for 7 d evaluated with DLS.

3.2. In vitro immune tolerance induction

Harnessing particle mediated spatiotemporal co-delivery has a pivotal role for modulating antigen-specific immunotolerance in that it can enhance antigen presentation efficiency of DCs, sequentially generate antigen-specific Tregs more efficiently. To verify effect of liposome nanoparticle delivery on antigen presentation efficiency of DCs, antigen location in DC was shown with confocal microscopy after L-Ag(FITC)/R treatment. DCs incubated with free Ag(FITC)/R displayed a weak intensity on plasma membrane at 6 h and the fluorescence became negligible after 24 h, whereas, by their high uptake efficiency, particle mediated delivered Ag(FITC)s were detected with strong signal in lysosome for 24 h and presented on cell membrane until 48 h (Fig. 3.2.A). For further validation, the augmented and sustained antigen presentation of DC was also evaluated with Yae antibody response (Fig. 3.2.B). Yae antibody can specifically bind to complex of Eα_{52-68}-MHC-II, allowing precise identification of antigen presentation of DC.[19] Similar to Fig. 3.2.A, The signal, positive to Yae antibody, was strong in plasma membrane of DC incubated with L- Eα/R compared to DC incubated with free Eα/R and lasted for a longer time when Eα was delivered with particle formulation (Fig. 3.2.C), which indicated that nanoparticle

mediated antigen delivery can establish robust and prolonged antigen presentation.

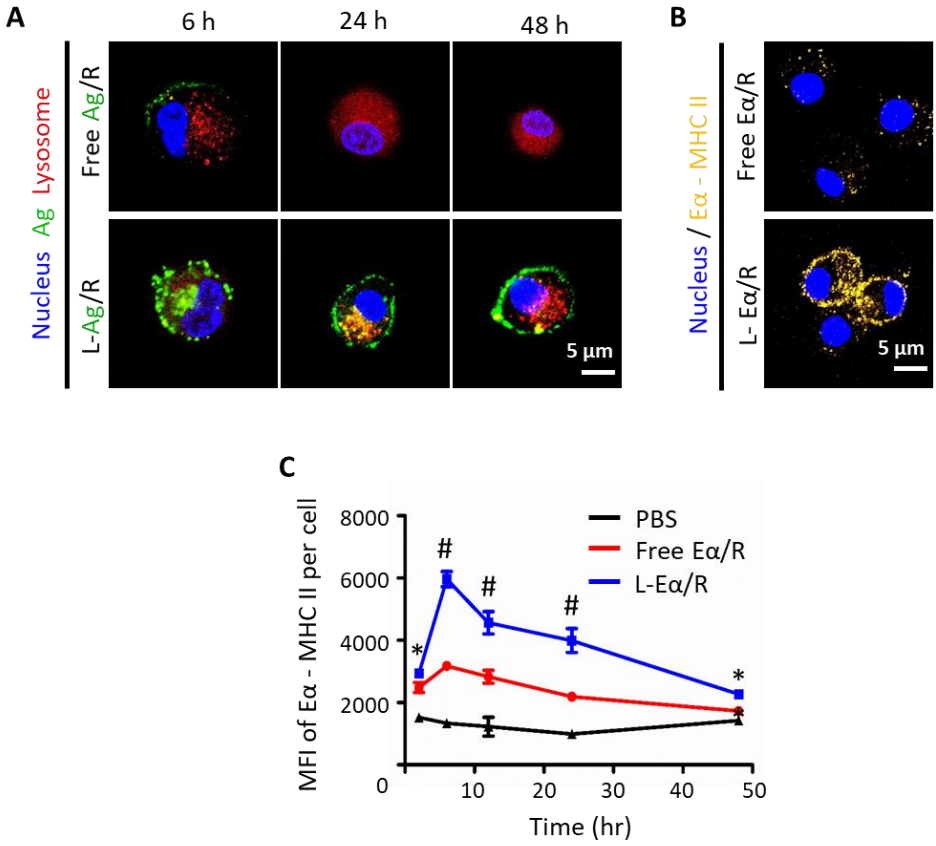

Figure 3.2. Liposome nanoparticle-mediated delivery of antigens enhances the antigen presentation efficiency of DCs. **A)** Confocal microscopic images sequentially showing antigen uptake by DC, antigen escape from lysosome, and antigen presentation on DC. **B)** Confocal microscopic images showing enhanced antigen presentation on MHC II of DCs by liposomal nanoparticle-mediated antigen delivery. DCs were treated with L-Eα/R or free Eα/R for 24 h; Eα served as an antigen. Eα peptides presented on MHC II of DCs were visualized with Yae antibodies that simultaneously bind to Eα peptides and MHC II. **C)** Flow cytometry analysis showing augmented

and prolonged antigen presentation by DCs in liposomal nanoparticle−mediated antigen delivery. $*P < 0.05$ vs. any group, $\#P < 0.001$ vs. any group. Statistical comparison was performed by two−way ANOVA

Next, to confirm a capability of L-Ag/R for eliciting immunotolerance in vitro, we investigated whether it can induce tolerogenic dendritic cell (tDC). After 48 h incubation with particle and additional 24 h LPS treatment, DCs treated with L-Ag/R showed lower levels of the co-stimulatory surface molecules (CD40, CD80, CD86) expression compared to Ag encapsulated liposome (L-Ag), LPS-derived mature DC (mDC) group owing to immunosuppressive effect of rapamycin (Fig. 3.3.A). Cytokine profile of DCs was also altered to promote anti-inflammatory responses, which is a characteristic of tDC (Fig. 3.3.B). With L-Ag/R treatment, mRNA levels of IFN-γ, TNF-α were increased when compared to imDC, however, were decreased compared with the other group, implying an ability of induced tDCs to resist an inflammatory signal. Contrary to the mRNA level of pro-inflammatory cytokines, substantial upregulation of mRNA levels of anti-inflammatory cytokines in L-Ag/R treated DC such as TGF-β, IL-10 was shown compared to other group (Fig. 3.3.C). Then, we performed a CFSE proliferation assay that CD4 T cells isolated from spleen of OT-II mice were labeled with CFSE and co-cultured for 5 days with the particle treated DCs. While a high degree of divided CD4 T cell population was shown in L-OVA treated DCs, L-OVA/R treated DCs suppressed the proliferation of the CD4 T cell (Fig. 3.3.D), which was in agreement with the characteristic of

tDC. These features including low expression of co-stimulatory molecules, mRNA of pro-inflammatory signal and poor T cell stimulatory capacity indicated that L-Ag/R can endow DCs with tolerogenic phenotype.

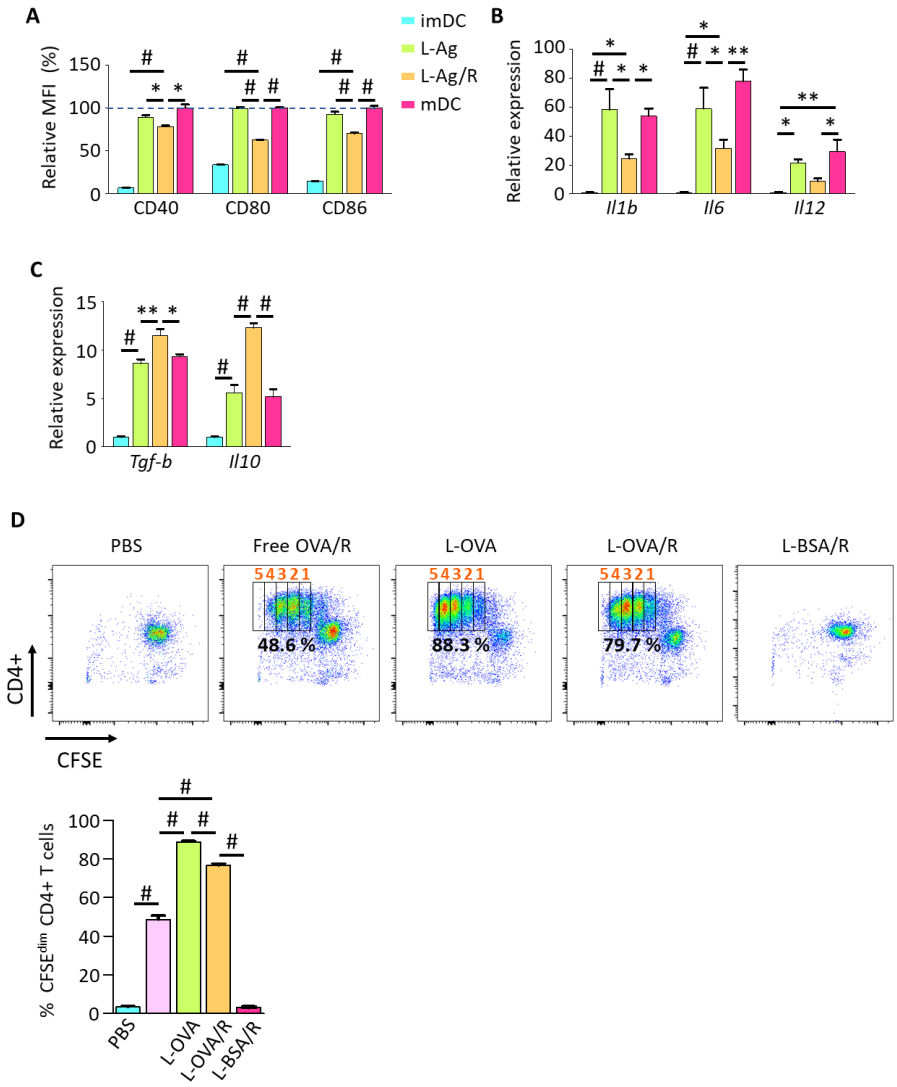

Figure 3.3. Co-delivery of antigens and rapamycin with liposome nanoparticles effectively induces tDCs. **A)** Expression of co-stimulatory surface molecules (CD40, CD80, and CD86) on DCs following different treatments, as evaluated by flow cytometry (n = 5 per group). **B)** mRNA levels of pro-inflammatory cytokines in DCs following different treatments, as evaluated by qRT-PCR (n = 7 per group). **C)** mRNA levels of anti-inflammatory cytokines in DCs

following different treatments, as evaluated by qRT-PCR (n = 5 per group). D) Representative flow cytometry dot plots and quantification of CFSEdim OT-II CD4+ T cells following co-culture with different DCs for 5 d. DCs were incubated with either free OVA/R, L-OVA, or L-OVA/R for 2 h, followed by LPS treatment for 1 h and co-culture with CD4+ T cells (n = 7 per group). *P < 0.05, **P < 0.01, #P < 0.001

Following the tDC induction with L-Ag/R, capability of the induced tDC to generate regulatory T cell (Treg), a key regulator of immune tolerance, was analyzed. Cocultured with L-OVA/R treated DCs for 5 days, proportion of the induced Foxp3+ T cells was shown to be the highest (Fig. 3.4.A), and tolerogenicity of Treg, as evaluated at mRNA levels by qRT-PCR, was also upregulated (Fig. 3.4.B), demonstrating the ability of L-Ag/R to provoke immune cascade response such as induction of tDC and Treg. With its high antigen presentation efficiency and capability of Treg generation, L-OVA/R nanoparticle generated antigen-specifc Treg efficiently. Different to free Ag/R treatment, the nanoparticle mediated spatiotemporal co-delivery of Ag and rapamycin enable DCs to both present antigen and differentiate to tDC simultaneously, which can make naive T cell to both be primed with specific antigen and have a tolerogenicity at the same time.

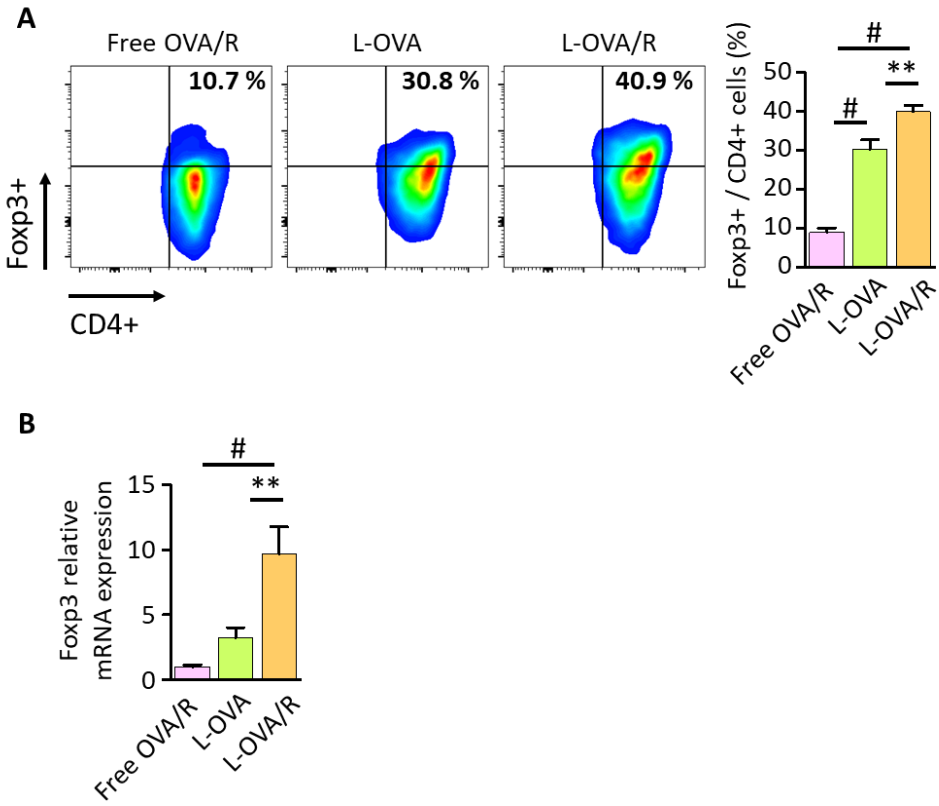

Figure 3.4. Co-delivery of antigens and rapamycin with liposome nanoparticles effectively induces antigen-specific Tregs. **A)** Flow cytometry analysis and quantification showing effective induction of OVA-specific Tregs by liposomal nanoparticle-mediated co-delivery of $OVA_{323-339}$ antigen and rapamycin. DCs were incubated with free OVA/R, L-OVA, or L-OVA/R for 2 h, followed by LPS treatment for 1 h. OVA-specific Tregs were induced by co-culture for 4 d with DCs treated with different nanoparticle formulations and $CD4^+$ T cells purified from splenocytes of OT-II mice (n = 7 per group); **B)** Foxp3 relative mRNA expressions in OT-II $CD4^+$ T cells

co-cultured with different DCs for 5 d, as evaluated by qRT-PCR (n = 7 per group). **P < 0.01, #P < 0.001

3.3. In vivo immune tolerance induction

Next, the formulated particles were injected intradermally near the left inguinal lymph node (iLN) to induce the immunotolerance in vivo through Treg, M2 modulation for ameliorating heart function. A day after intradermal injection, Cy5.5-labeled L-Ag/Rs accumulated at the iLN (Fig. 3.5.A), and were shown to be colocalized with CD11c+ DC (Fig. 3.5.B). Assuming that the diameter of L-Ag/R (~200 nm) is too large to be delivered to lymph node directly, L-Ag/Rs would have been transfered to the iLN via DCs that internalized L-Ag/R. As shown Figure 3.2, DCs that uptake L-Ag/R may regulate microenvironment in lymph node towards tolerance, so we examined variation of Treg population in the draining lymph node 5 days after treatment by flow cytometry. In the left iLN, the population of CD25+Foxp3+ CD4 Tregs in L-Ag/R treated mice was enhanced compared to the other group (Fig. 3.5.C), which suggested that the L-Ag/R uptaked DCs exhibited a tolerogenic effect to the lymph node microenvironment. Interestingly, the population of Treg at spleen was also increased, indicating that the modulation of local immune environment can lead to elicitation of systemic immunotolerance, as reported previously.[20]

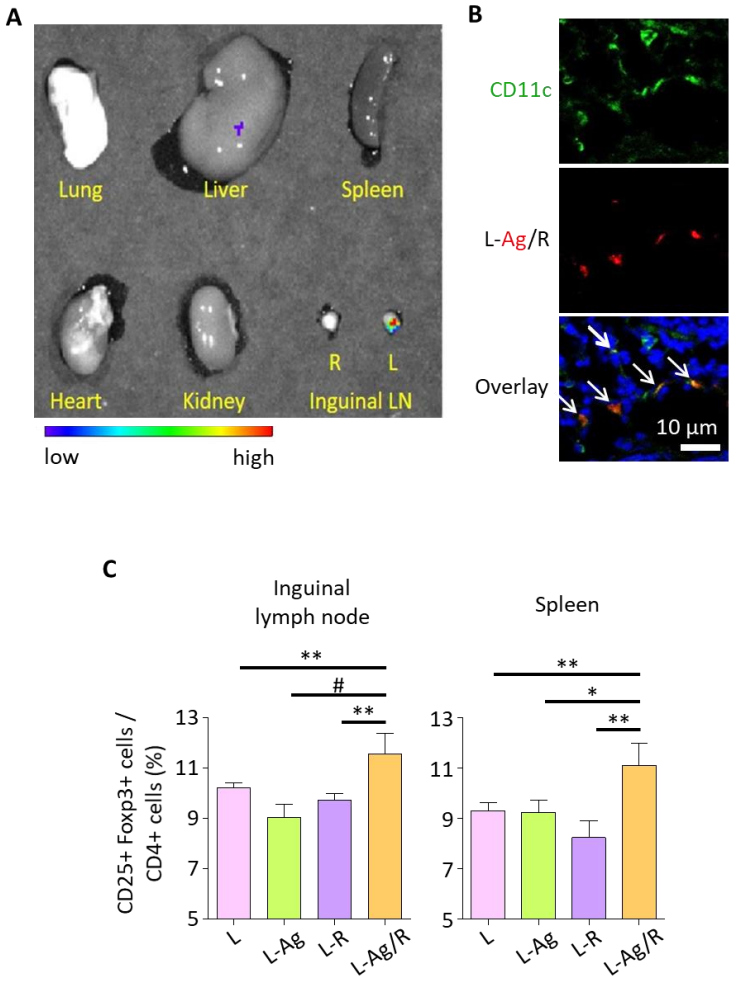

Figure 3.5. Intradermal injection of L−Ag/R into MI mice induces Tregs systemically. L−Ag/R nanoparticles were intradermally injected near the left inguinal lymph node (iLN). **A)** IVIS image showing biodistribution of fluorescence−labeled L−Ag/R 1 d after administration. **B)** Immunostaining of iLN 1 d after nanoparticle injection. Arrows indicate L−Ag/R uptake by $CD11c^+$ DCs in iLN. The antigens were conjugated with Cy5.5 (red) prior to injection. **C)** $CD25^+Foxp3^+$ (Treg) proportion in $CD4^+$ T cells in left iLN and

spleen 5 d after nanoparticle injection, as evaluated by flow cytometry (n = 7–10 per group). Data represent average ± SEM. $*P < 0.05$, $**P < 0.01$, $\#P < 0.001$ using one-way ANOVA followed by Newman-Keuls multiple comparison test.

Then, to investigate change of immune environmet at the infarcted heart, immunohistological staining with Treg, M1 and M2 marker was performed. Compared to the other group, L-Ag/R treated mice displayed the highest absolute number of Foxp3+ Treg and CD206+ M2 macrophage at the border zone, and on the contrary, the number of iNOS+ M1 macrophage was the lowest (Fig. 3.6). The data showed that function of Treg was the strongest in L-Ag/R treated group because macrophage phenotype shift from M1 to M2 is closely related to Tregs that can promote M2 macrophage polarization and suppress inflammatory cells including M1 macrophage and cytotoxic T cell. Ascribed to function of antigen-specific Tregs and M2 polarization, mRNA levels of pro-inflammatory cytokines were downregulated while that of anti-inflammatory cytokines were upregulated (Fig. 3.7), which can inhibit adverse cardiac remodeling and facilitate cardiac repair.

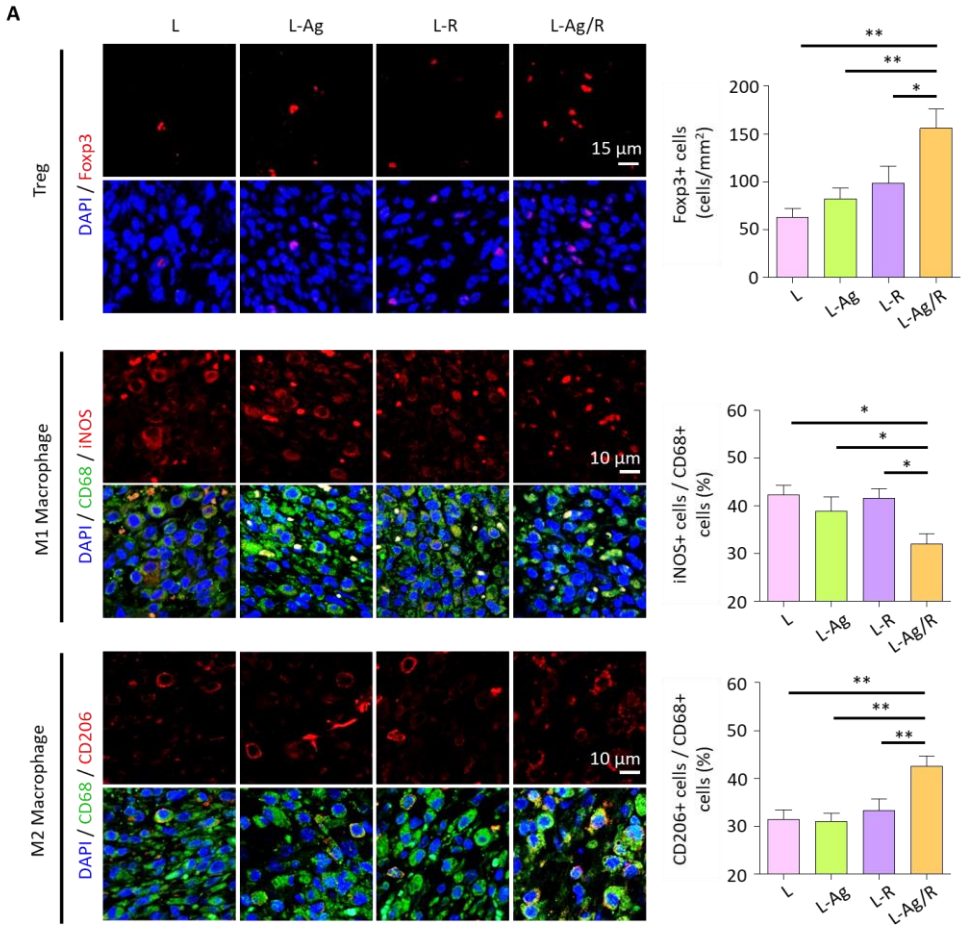

Figure 3.6. Representative confocal microscopic images of Tregs, M1 macrophages, and M2 macrophages in the infarct zone of infarcted myocardium 5 d after nanoparticle injection. Tregs were stained with anti-Foxp3 (red). M1 macrophages were stained with anti-CD68 (green) and anti-iNOS (red). M2 macrophages were stained with anti-CD68 (green) and anti-CD206 (red). Data represent average ± SEM. $*P < 0.05$, $**P < 0.01$, $\#P < 0.001$ using one-way ANOVA followed by Newman-Keuls multiple comparison test.

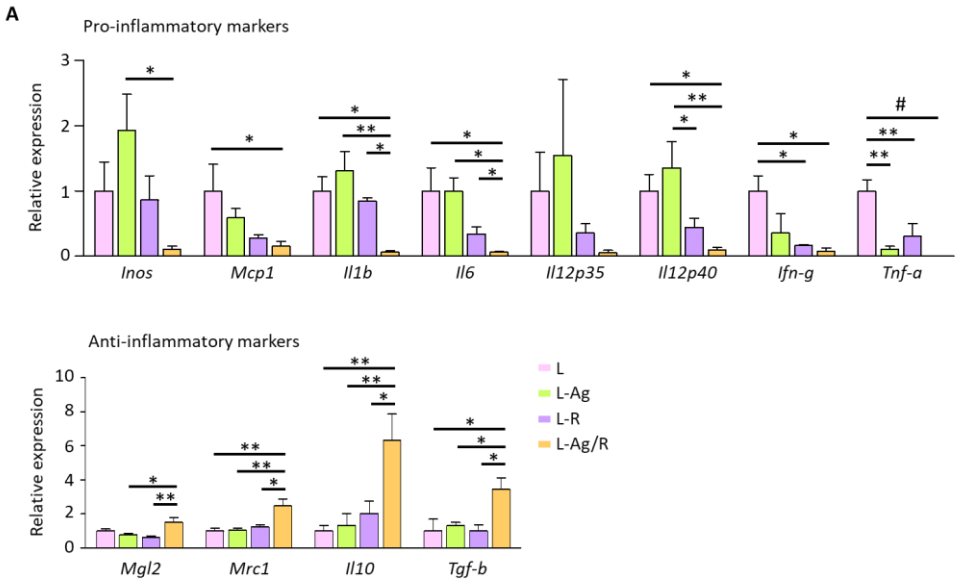

Figure 3.7. mRNA expression of pro-inflammatory and anti-inflammatory markers in MI region of infarcted myocardium 5 d after nanoparticle injection (n = 3–5 per group). Data represent average ± SEM. $*P < 0.05$, $**P < 0.01$, $\#P < 0.001$ using one-way ANOVA followed by Newman-Keuls multiple comparison test.

3.4. Improved cardiac function by nanoparticle treatment

To investigate the cardioprotective effects of L−Ag/R on MI hearts, L, L−Ag, L−R and L−Ag/R were intradermally injected once a week for 2 weeks after induction of MI by LAD ligation. We assessed structural changes in LV structure at 28 days after MI and performed histological evaluation using Masson’s trichrome staining. The L−Ag/R−treated group showed a significant reduction in the infarct size and less fibrosis compared with the other groups (Fig. 3.8.A,B). Cardioprotective effect of L−Ag/R treatment in inhibition of capillary vessel destruction and cardiac cell death were also observed by CD31, TUNEL staining, respectively (Fig. 3.9.A,B). Furthermore, we examined the changes in LV function of infarcted hearts, evaluated by M−mode echocardiographic assessment of LV function at 28 days after MI (Fig. 3.10.A,B). Both EF (38.2 ± 4 % vs. 23.1 ± 5%) and FS (16.5±2 % vs. 8.9 ± 2 %) were significantly higher in L−Ag/R treated mice than the free liposome treatment group. Similarly, a significant decrease in ESV by 48.5 % was observed in the L−Ag/R treatment group (0.16 ± 0.05 mL) compared to the control free other treatment group. The mice treated with either the L−Ag or L−R showed significant improvement in EF, FS, and ESV, and the greater effects on preserving LV systolic function were observed in

the L−Ag/R treatment group than that occurring in the other groups. Taken together, these results clearly suggest that L−Ag/R treatment induced less LV dilation and deterioration in LV contractility after myocardial infarction, indicating its therapeutic potential to reduce post−infarct adverse remodeling and cardiac dysfunction

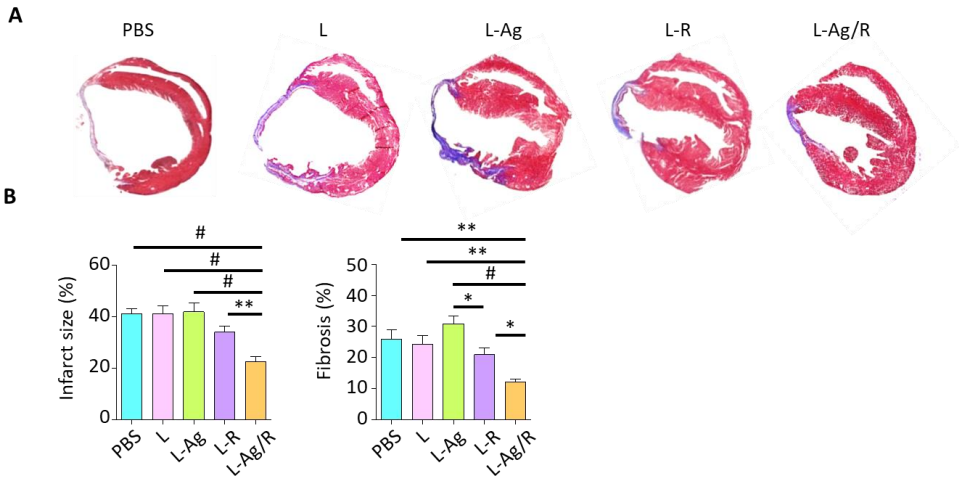

Figure 3.8. Intradermal injection of L−Ag/R into MI mice inhibits adverse cardiac remodeling and improves cardiac function. **A)** Representative Masson' s trichrome staining images of MI heart tissues sectioned at the level of papillary muscles 28 d after nanoparticle injection. **B)** Quantification of infarct size (left) and fibrosis area (right) in the infarcted hearts (n = 5–10 animals per group). Data represent average ± SEM. *P < 0.05, **P < 0.01, #P < 0.001 using one−way ANOVA followed by Newman–Keuls multiple comparison test.

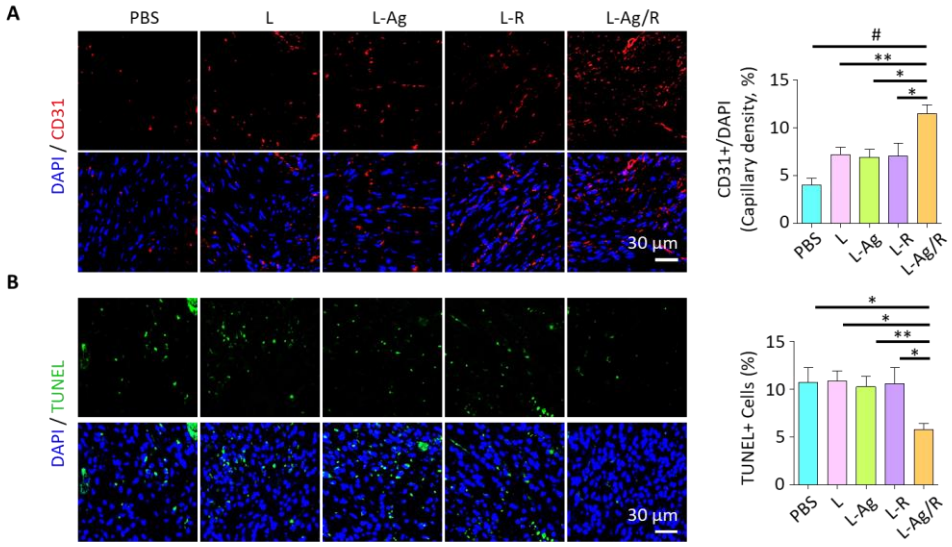

Figure 3.9. Intradermal injection of L-Ag/R into MI mice inhibits capilary vessel destruction and cardiac cell apoptosis. **A)** Representative confocal microscopic images of CD31-positive (red) endothelial cells in the infarct zone 5 d after nanoparticle injection (n = 5-7 animals per group). **B)** Representative confocal microscopic images of TUNEL positive (green) apoptotic cells in the infarct zone 5 d after nanoparticle injection (n = 7-11 animals per group). Data represent average ± SEM. *P < 0.05, **P < 0.01, #P < 0.001 using one-way ANOVA followed by Newman-Keuls multiple comparison test.

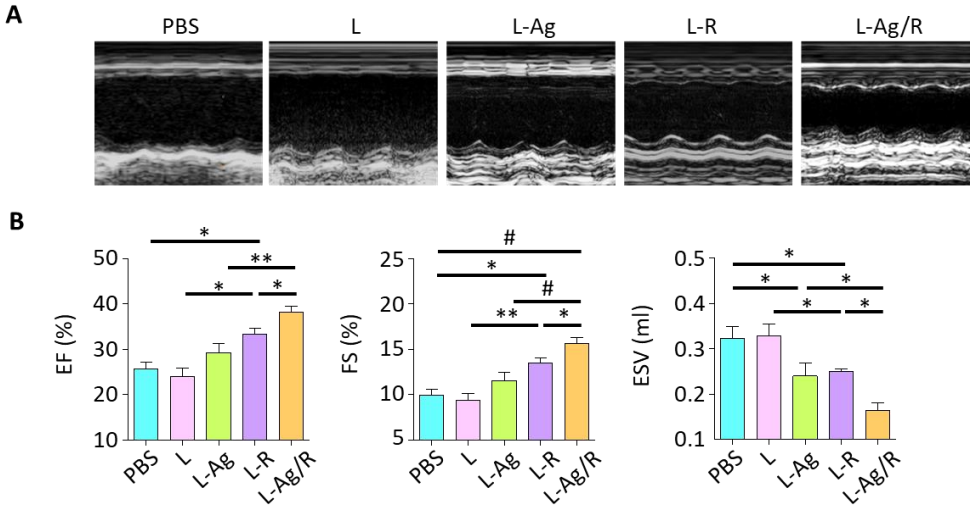

Figure 3.10. Intradermal injection of L−Ag/R into MI mice prevent cardiac function deteoration. **A)** Representative M−mode echocardiography images 28 d after MI. **B)** Quantification of ejection fraction (EF), fractional shortening (FS), and end−systolic volume (ESV) (n = 5–10 animals per group). Data represent average ± SEM. *P < 0.05, **P < 0.01, #P < 0.001 using one−way ANOVA followed by Newman–Keuls multiple comparison test.

Chapter 4. Nanothin, nanoporous PLGA membrane for direct reprogramming of fibroblast and evaluation of drug-induced cardiotoxicity

4.1. PLGA membrane characterization and cardiac-mimetic cell induction

The GMTHM-transfected cells were positive to GFP, which indicated that the transfection was successfully conducted (Fig. 4.1.A) and reached to ~ 20% (Fig. 4.1.B). The morphology of GMTHM-transfected cells was obtained using microscopy. The morphology of the cells plated on the PLGA membrane was similar to that of the cell plated on common culture dish (Fig. 4.1.C). After 7 days of GMTHM transfection, cardiac mRNAs in early cardiac development stage were increased, suggesting that cardiac features were endowed by GMTHM transfection (Fig. 4.1.D). The GMTHM-transfected cells were cultured on PLGA nano-porous thin membrane. The PLGA membranes were fabricated with spin coating method, and AFM images showed the increasing pore size from 300 nm to 600 nm over time from 1 to 4 weeks (Fig. 4.1.E).

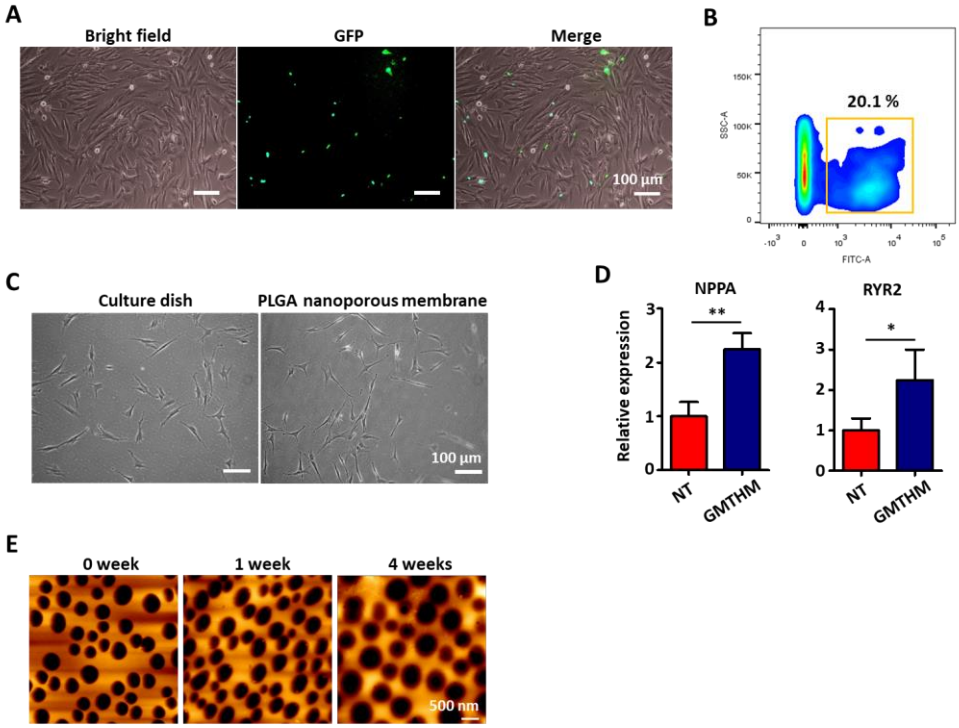

Figure 4.1. Cardiac reprogramming of human neonatal dermal fibroblasts (HNDFs). A) Fluorescence microscopic images and B) flow cytometry analysis for detecting GFP-positive cells after transfection of cardiac reprogramming factors, GMTHM. C) Morphology of transfected HNDFs plated on culture dish and PLGA nano-porous membrane. D) Cardiac mRNA expression 7 days after GMTHM transfection. Data are average ± SD. *P < 0.05, **P < 0.01. Statistical significance was determined using unpaired t-test. E) Morphology and pore size variation of PLGA nano-porous membranes following incubation in culture medium for various time periods.

4.2. Double-layered cell sheet construction

Double-layered, cardiac reprogrammed cell sheets were constructed by stacking two the nanoporous PLGA membrane, which contained the cardiac-mimetic cell, through layer-by-layer (LbL) technique and incubated for 7 days. To investigate the close proximity of each sheets, the cardiac-mimetic cells on the membrane were pre-labelled with DiD or DiO, and then constructed to double layer. Confocal microscopic image showed that the cardiac reprogrammed cells, which were cultured on the PLGA membrane, were closely contact each other (Fig. 4.2.A). Further, histological staining of the mono or double layer demonstrated that LbL method established double-layered, cardiac-mimetic cell sheet, showing that the thickness of mono and double layer was 23.6 ± 1.2 μm, and 40.8 ± 3.2 μm, respectively (Fig. 4.2.B). The double-layered, cardiac-mimetic cells expressed cTNT, cardiomyocyte marker, and cardiac-related gene expressions were also augmented compared to HNDFs (Fig. 4.2.C, D).

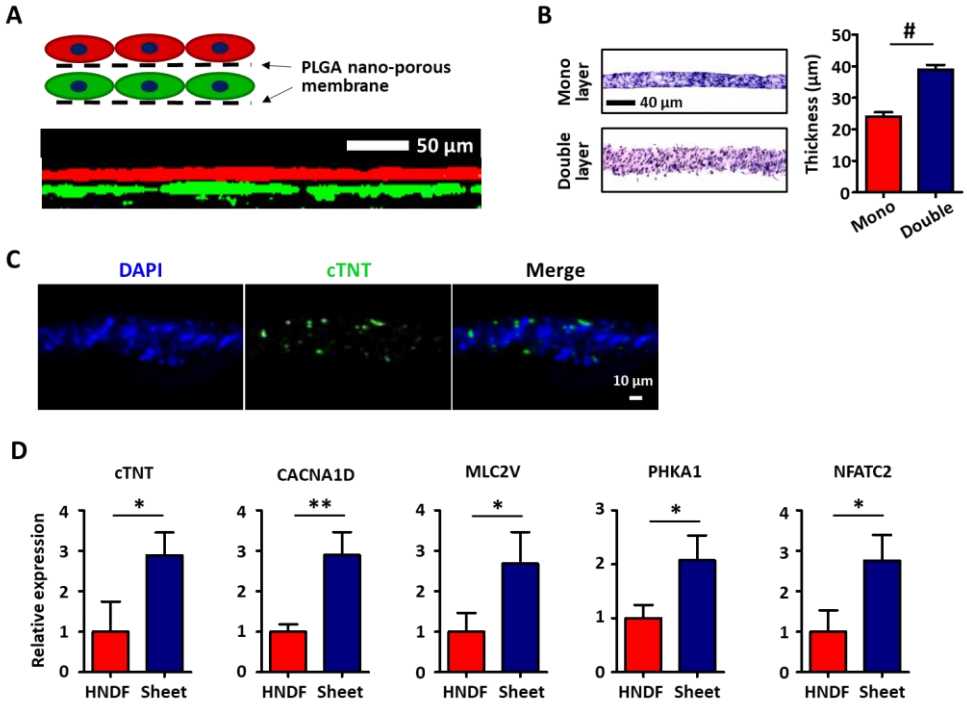

Figure 4.2. Characterization of double layered, cardiac reprogrammed cell sheet. A) A side view of fluorescent microscopic image of double layer stacking of DiD (upper, red) – and DiO (bottom, green) –labelled cardiac reprogrammed cell sheets. B) Histological images and thickness of monolayer and double layer cell–sheet of cardiac reprogrammed cells. n = 3 per group. C) Immunocytochemistry showing cTnT expression in double layered cardiac reprogrammed cell sheets. D) Cardiac mRNA expressions in HNDFs and double layered cardiac reprogrammed cell sheets. Data are average ± SD. *P < 0.05, **P < 0.01, #P < 0.001. Statistical significance was determined using unpaired t–test.

4.3. Enhanced resistance to drug by 3D organization

Next, we examine the effect of the cell layer number on cytotoxicity of 5-FU. After 1mM 5-FU treatment for 72 h, normalized percentage of Annexin V-positive cells was lower in double layer than mono layer (Fig. 4.3.A). Furthermore, Bcl-2/Bax expression ratio was enhanced by constructing double-layered sheet, suggesting that the double-layered structure exhibit higher drug resistance than the monolayer (Fig. 4.3.B). 5-FU can deteriorate mitochondrial function and subsequently trigger lipid peroxidation in cell membrane.[21-23] To further investigate the drug resistance resulted from the double-layered structure, C11-BODIPY was used to stain cell membrane and verify lipid peroxidation. Upon 5-FU treatment for 72 h, fluorescence intensity of 591 nm emission wavelength weakened, meanwhile, that of 510 nm emission wavelength was not significantly altered (Fig. 4.3.C). The ratio of intensity from 510 nm emission wavelength and that from 591 nm emission wavelength was reduced, indicating that the double-layered cell sheet was more resistant to lipid peroxidation by 5-FU than mono-layered cell sheet (Fig. 4.3.D). In addition, mRNA expression of a senescence-associated gene and pro-inflammatory cytokine genes were inhibited, which can contribute to protective effect of

double-layered structure (Fig. 4.3.E).

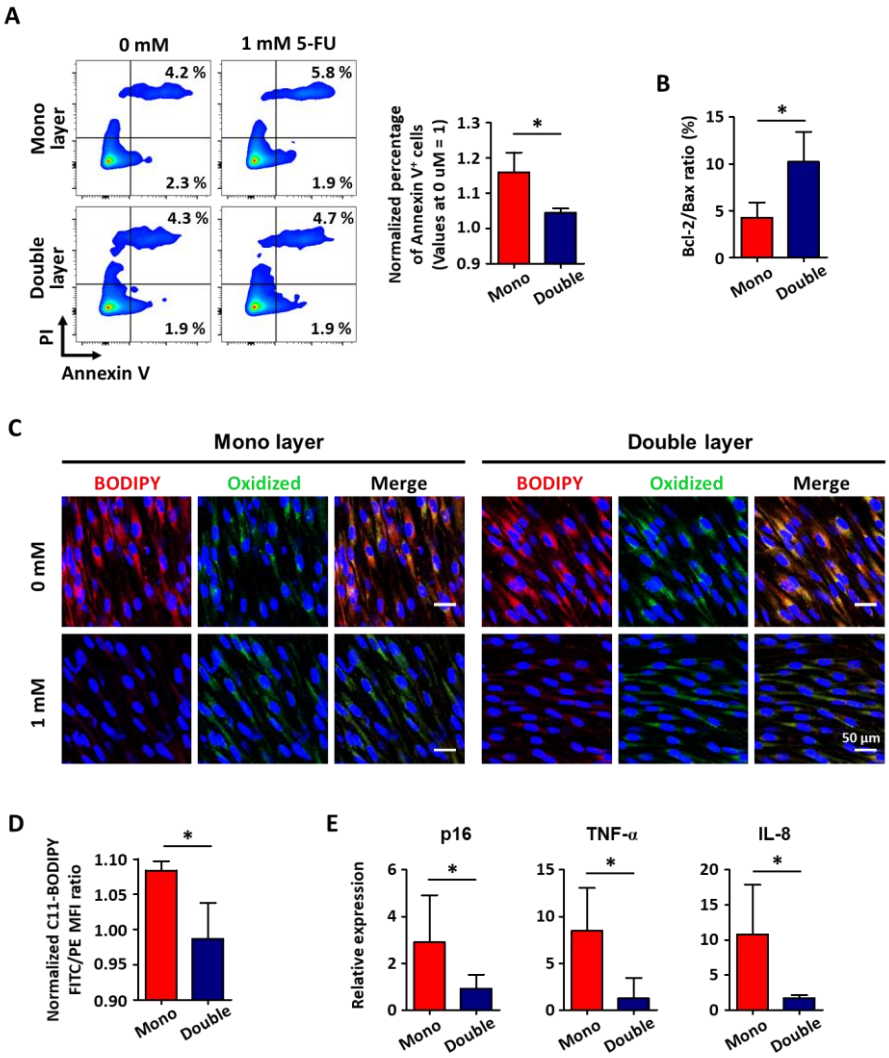

Figure 4.3. Cell sheet layer number-dependent cytotoxicity of 5-FU and lipid peroxidation in response to 5-FU in cardiac reprogrammed cell sheets. Mono- and double-layered cell sheets were incubated with 5-FU for 72 h. A) Cell sheet layer number-dependent cytotoxicity of 5-FU, as determined by apoptotic cell (Annexin V^+ cell) quantification using flow cytometry. B) Bcl-2/Bax mRNA expression ratio of mono and double layered cardiac reprogrammed

cell sheets in response to 5-FU (1 mM). C) Cell sheet layer number-dependent lipid peroxidation, as analyzed with confocal microscopy. Cell membranes were stained with C11-BODIPY (red) and were oxidized (green) by 5-FU treamtment. D) Cell sheet layer number-dependent lipid peroxidation in response to 5-FU (1 mM), as evaluated with flow cytometry. E) Cell sheet layer number-dependent mRNA expressions of a senescence-associated gene (p16) and pro-inflammatory cytokine genes (TNF-α and IL-8) in response to 5-FU (1 mM). Data are average ± SD. *P < 0.05. Statistical significance was determined using unpaired t-test.

4.4. Drug-induced cardiotoxicity evaluation

To further evaluate cell sheet layer number-dependency on drug resistance, we analyzed mitochondrial dysfunction and cell membrane permeability using high content analysis (HCA). Used to assess structural cardiotoxicity, HCA can evaluate mitochondrial membrane potential ($\Delta\Psi m$), ER integrity, calcium ion concentration, and cell permeability (Plasma membrane; PM). In this study, we measured mitochondrial membrane potential by TMRE and cell membrane permeability by TOTO-3 because 5-FU can harm mitochondrial function.[21,22] The cardiac-mimetic cells were stained with TMRE, TOTO-3, and hoechst 33342, and then fluorescence microscopic images were obtained. In contrast to mono-layered cell sheet, double-layered cell sheet retained higher mitochondrial membrane potential at 1 μM 5-FU, demonstrating that double-layered cell sheet tolerated toxicity of 5-FU and maintained mitochondrial function (Fig. 4.4.A). Lower TOTO-3 positive cells were shown in double-layered cell sheet than mono-layered cell sheet at 1 mM, suggesting that the cells on double layer had a more intact cell membrane, which can lead to higher cell viability. At mitochondrial membrane potential, the IC50 of the mono and the double layer were estimated to be 8.6 μM and 0.1 mM, respectively (Fig. 4.4.B).

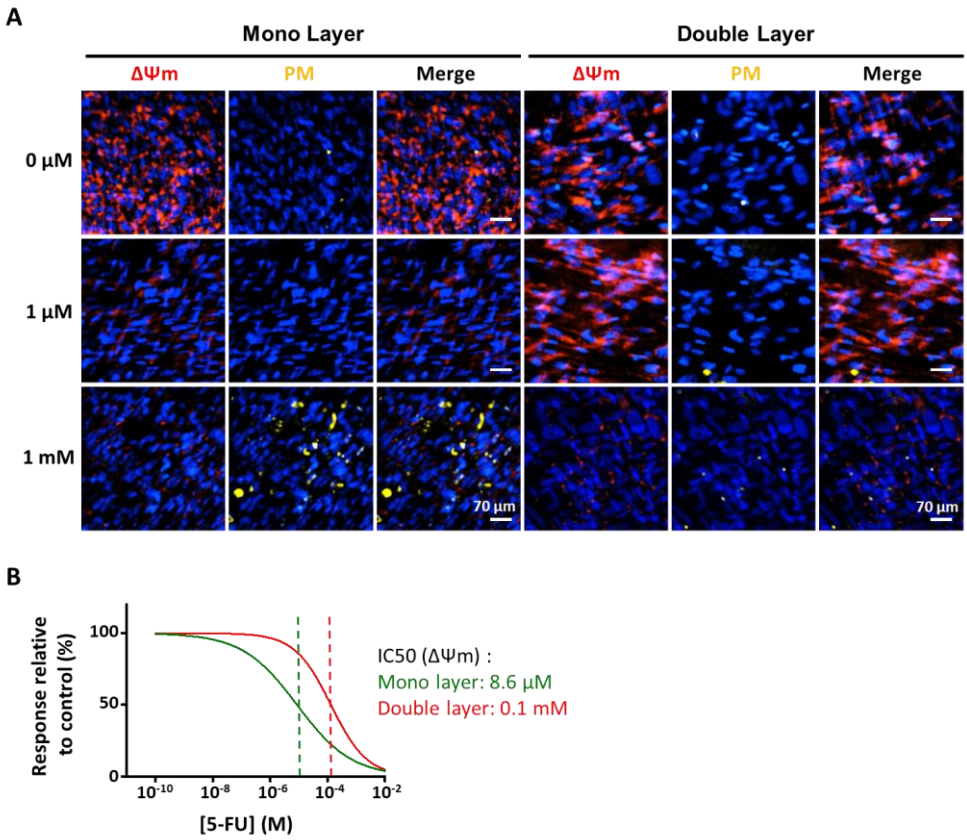

Figure 4.4. Cell sheet layer number-dependent cardiotoxicity of 5-FU in cardiac reprogrammed cell sheets. **A)** Cell sheet layer number-dependent cytotoxicity of 5-FU, as determined by high content analysis. Cell sheet layers are stained with Hoechst 33342 (Nucleus, blue), TMRM(⊿Ψm, red), and TOTO-3 (PM, yellow). **B)** 5-FU drug-responsiveness profiles of mono- or double-layered cardiac reprogrammed cell sheet.

4.5. Enhanced resistance to drug by cell density

Intrigued by drug resistance of cardiac-mimetic cells to 5-FU, which was dependent on cell sheet number, we investigated whether cell density affects to cytotoxicity and lipid peroxidation in 2D culture system. Trypsinized cardiac-mimetic cells were seeded at 1.25 x 10^2, 5 x 10^2, and 1.25 x 10^3 cells/mm^2 and treated with different concentration of 5-FU. As shown in Fig. 4.5.A, Proportion of Annexin V-positive cells increased with increasing concentration of 5-FU, but the tendency became negligible with higher cell density, providing evidence that high cell density can inhibit apoptosis of the cardiac-mimetic cells. Cell viability analyzed using CCK assay also indicated that drug resistance was enhanced when cell density was high (Fig. 4.5.B). To further evaluate effect of cell density on cellular toxicity, lipid peroxidation using C11-BODIPY was conducted. With the similar trend to the drug resistance in apoptosis by 5-FU, lipid peroxidation, which was measured by MFI of FITC/PE using flow cytometry, was suppressed when cell density became higher (Fig. 4.5.C).

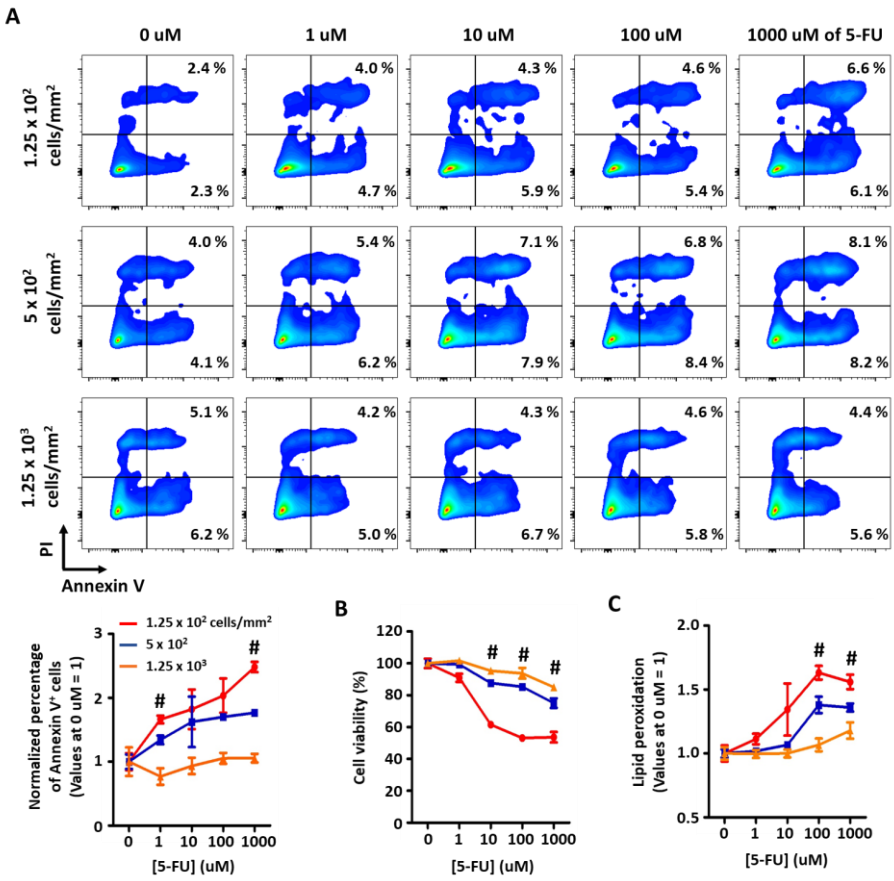

Figure 4.5. Cell density-dependent cytotoxicity and lipid peroxidation in monolayer cultures of cardiac reprogrammed cells following treatment with various concentrations of 5-FU. Different concentration of the cells were incubated with 5-FU for 72 h A) Cell density-dependent apoptosis (Annexin V^+ cells) in response to 5-FU, as determined by apoptosis analysis using flow cytometry. (B) Cell density-dependent viability of cells treated with 5-FU, as analyzed by CCK-8 assay. C) Cell density-dependent lipid peroxidation in cells treated with 5-FU, as expressed with MFI of FITC/PE following C11-BODIPY staining. Data are average ± SD.

# $P < 0.001$ versus any group. Statistical significance was determined using one-way ANOVA followed by Newman-Keuls multiple comparison test.

Chapter 5. Conclusion

Intradermal injection of L-Ag/R enabled spatiotemporal co-delivery of antigens and rapamycin to DCs. The nanoparticle-mediated delivery elicited a robust and finely precise immune tolerance by inducing antigen-specific Tregs. Consequently, L-Ag/R inhibited the adverse cardiac remodeling and improved the cardiac function in MI animal models. The immune-modulating nanoparticle strategy may have a high therapeutic value for prevention of post-MI heart failure and contribute to advancement of MI treatment.

Using nanothin, nanoporous PLGA membranes, I directly reprogrammed HNDFs to induce cardiac-mimetic cells. Combining both reprogramming technique and constructing 3D structure through LbL method can contribute to producing a research model in drug-induced toxicity. Our platform in this study can be useful tool to construct multiple-layered cell sheet that can mimic in vivo 3D structure and spatial compactness of cells.

In conclusion, nanomaterials can contribute to predicting and preventing heart failure and provide opportunity to approach clinical application.

Reference

[1] A. Torabi, A. S. Rigby, J. G. Cleland, *J Am Coll Cardiol* 2009, *55*, 79.

[2] A. M. van der Laan, M. Nahrendorf, J. J. Piek, *Heart* 2012, *98*, 1384.

[3] S. D. Prabhu, N. G. Frangogiannis, *Circulation research* 2016, *119*, 91.

[4] S. M. Parizadeh, R. Jafarzadeh-Esfehani, M. Ghandehari, M. R. Parizadeh, G. A. Ferns, A. Avan, S. M. Hassanian, *J Cell Physiol* 2019, *234*, 16904.

[5] E. H. Choo, J. H. Lee, E. H. Park, H. E. Park, N. C. Jung, T. H. Kim, Y. S. Koh, E. Kim, K. B. Seung, C. Park, K. S. Hong, K. Kang, J. Y. Song, H. G. Seo, D. S. Lim, K. Chang, *Circulation* 2017, *135*, 1444.

[6] K. Matsumoto, M. Ogawa, J.-i. Suzuki, Y. Hirata, R. Nagai, M. Isobe, *International heart journal* 2011, *52*, 382.

[7] J. Weirather, U. D. Hofmann, N. Beyersdorf, G. C. Ramos, B. Vogel, A. Frey, G. Ertl, T. Kerkau, S. Frantz, *Circulation research* 2014, *115*, 55.

[8] R. Duggleby, R. D. Danby, J. A. Madrigal, A. Saudemont, *Front Immunol* 2018, *9*, 252.

[9] S. N. Furlan, K. Singh, C. Lopez, V. Tkachev, D. J. Hunt, J. Hibbard, K. M. Betz, B. R. Blazar, C. Trapnell, L. S. Kean, *Blood Adv*

2020, *4*, 1594.

[10] B. E. Phillips, Y. Garciafigueroa, C. Engman, M. Trucco, N. Giannoukakis, *Front Immunol* 2019, *10*, 148.

[11] S. Y. Song, H. Kim, J. Yoo, S. P. Kwon, B. W. Park, J. J. Kim, K. Ban, K. Char, H. J. Park, B. S. Kim, *Biomater Sci* 2020, *8*, 4508.

[12] S. Y. Song, J. Yoo, S. Go, J. Hong, H. S. Sohn, J.-R. Lee, M. Kang, G.-J. Jeong, S. Ryu, S. H. L. Kim, *Theranostics* 2019, *9*, 6734.

[13] G. Gintant, P. Burridge, L. Gepstein, S. Harding, T. Herron, C. Hong, J. Jalife, J. C. Wu, A. H. A. C. o. B. C. Sciences, *Circulation research* 2019, *125*, e75.

[14] S. L. Murphy, K. D. Kochanek, J. Xu, M. Heron, *Natl Vital Stat Rep* 2015, *63*, 1.

[15] H. Laverty, C. Benson, E. Cartwright, M. Cross, C. Garland, T. Hammond, C. Holloway, N. McMahon, J. Milligan, B. Park, *British journal of pharmacology* 2011, *163*, 675.

[16] M. B. Lutz, N. Kukutsch, A. L. Ogilvie, S. Rossner, F. Koch, N. Romani, G. Schuler, *J Immunol Methods* 1999, *223*, 77.

[17] M. Frohlich, V. Brecht, R. Peschka-Suss, *Chem Phys Lipids* 2001, *109*, 103.

[18] R. K. Nukala, H. Boyapally, I. J. Slipper, A. P. Mendham, D. Douroumis, *Pharm Res* 2010, *27*, 72.

[19] Y. Rudensky, P. Preston-Hurlburt, S. C. Hong, A. Barlow, C.

A. Janeway, Jr., *Nature* 1991, *353*, 622.

[20] L. H. Tostanoski, Y. C. Chiu, J. M. Gammon, T. Simon, J. I. Andorko, J. S. Bromberg, C. M. Jewell, *Cell Rep* 2016, *16*, 2940.

[21] H. A. Deveci, M. Nazıroğlu, G. Nur, *Molecular and cellular biochemistry* 2018, *439*, 189.

[22] M. Koçer, M. Nazıroğlu, *Biological trace element research* 2013, *155*, 327.

[23] F. M. Santandreu, A. Valle, J. Oliver, P. Roca, *Cellular Physiology and Biochemistry* 2011, *28*, 219.

요약

심근 경색증은 약물 유발 성 심장 독성을 비롯한 다양한 문제로 인해 발생할 수 있다. 경색 후 심각한 심장 손상은 과도한 염증을 일으켜 조직 손상을 유지하고 종종 심장 기능 손상 및 심부전, 그리고 심장 협착증을 악화시킨다. 적시에 염증을 진료하여 심부전 발생을 예방하거나 약물의 심독성을 측정할 수 있는 방법이 논의되어야 한다.

나노 물질은 치료 및 진단과 같은 생물학적 응용 분야에서 높은 잠재력을 가진다. 그 중에서도 나노 입자는 약물이나 생체 분자를 전달하기 위해 널리 사용되는 제형이다. 나노 제형은 1) 손쉬운 표면 개질, 2) 인체 내 효소에 의한 약물 분해 차단, 3) 입자의 나노 크기에 의해 촉진되는 세포와의 상호 작용에 유리하며, 이 모든 것이 입자 특성 제어 및 효율적인 약물 전달을 가능하게 한다. 나노 물질이 심부전 예방에 많은 장점과 잠재력을 가지고있는 것으로 예상되나, 나노 기술의 심근경색 치료나 독성측정에 대한 연구는 진전이 미비하다.

본 연구는 심근경색 치료 및 약물 유발성 심장독성 평가에서 나노 물질의 장점을 제시한다. 첫째, L-Ag / R (항원 및 라파마이신이 탑재된 리포좀)의 피내 주사는 항원과 라파마이신을 수지상 세포로의 효과적인 전달을 가능하게 하여 면역관용 및 심장 기능을 향상시켰다. 둘째, 나노 다공성, 나노 박막 PLGA 멤브레인 기반의 세포 배양 플랫폼을 통해 약물 유발성 심장독성에 영향을 미치는 잠재적인 요소를 찾을 수 있다. 개발된 플랫폼은 약물 독성 예측의 정확성을 향상시킬 수 있다. 따라서, 나노 물질은 심부전을 예방하거나 심독성을 측정하는데 기여할 수 있으며, 임상 적용으로의 기회를 제공 할 것이다.

주요어: 나노재료, 나노의학, 심근경색, 약물 유발성 심장독성

학번: 2016-33931